International Ultraviolet Association
6935 Wisconsin Avenue, Suite 207
Chevy Chase, MD 20815
www.iuva.org

Far UV-C Radiation: Current State-of Knowledge

Any opinions, findings, and conclusions or recommendations expressed in this material are those of the authors and do not necessarily reflect the views of the International Ultraviolet Association.

Executive Summary

The COVID-19 pandemic has heightened awareness of the risks associated with disease transmission by surface- and, particularly, airborne-associated pathogens; this risk awareness brings a desire for solutions. UV-C radiation (at shorter wavelengths outside the visible spectrum) has been employed for air and surface disinfection since the 1940's. There is unequivocal evidence that UV-C can be used to reduce the incidence of communicable diseases transmitted via fomites and by airborne droplets or aerosols across a range of settings. UV-C disrupts the reproductive cycle of the targeted pathogens, rendering them inactive. Further, recent studies have conclusively shown that UV-C rapidly inactivates SARS-CoV-2, the virus that causes COVID-19, as well as other common airborne pathogens such as influenza viruses.

Far UV-C radiation (200-230 nm) is a region of the UV-C spectrum not traditionally used for disinfection, though it has been known to be an effective antimicrobial and antiviral agent. The significance of Far UV-C is that, whereas exposure to conventional germicidal UV (250-280 nm) at germicidal doses is potentially hazardous, biophysical and experimental evidence suggest this is not the case for Far UV-C; greater absorption by protective surface layers results much less damage to skin and eye, while maintaining disinfection efficacy. Thus Far UV-C offers the potential to fundamentally change how and where UV-C radiation can be used for surface and, particularly, airborne decontamination, opening the potential for its use in occupied spaces.

This White Paper is a scientific review of Far UV-C technology and the state of the art research; this, however, does not constitute a complete review of regulations around this technology, which may vary substantially region-to-region and by application. Key conclusions of this Report, made through analysis of published literature and collation of expert knowledge, are:

- Inactivation of viral pathogens by Far UV-C is at least, and often more effective as compared with conventional UV-C.
- There is no evidence, to date, of any adverse human eye or skin damage (including consideration of skin cancers) from Far UV-C delivered at relevant germicidal exposures.
- Far UV-C sources often emit potentially harmful radiation outside of the Far UV-C range, though at relatively lower intensity. Spectral characterization of Far UV-C sources is crucial when understanding their safety; sources with significant emission above 230 nm may require optical filtering.
- Ozone generation by some Far UV-C lamps has been observed and, though manageable, should be considered and measured during application design.

In summary, while research should continue into both the safety and efficacy of Far UV-C, the material in this Report suggests that there is sufficient evidence for immediate consideration of this technology during this world-wide health crisis. Far UV-C offers a promising technology to reduce surface and airborne disease transmission in occupied spaces, including COVID-19 and other viral diseases, when it is properly designed, engineered, and applied.

Scope

As part of its COVID-19 initiatives, the International Ultraviolet Association (IUVA) convened a Task Force (TF) to assemble a comprehensive summary of the current state-of-knowledge related to Far UV-C technologies for use in disinfection of air and surfaces. This summary addresses the antimicrobial and antiviral properties of Far UV-C radiation (with particular focus on antiviral behavior), the effects of Far UV-C radiation on mammalian tissues, and the potential for formation of ozone by Far UV-C devices. In a broader sense, this document is intended to provide a summary of what we know and what we do not know about Far UV-C radiation and its application in practical settings. The aggregation of knowledge in this document may be used to inform decisions regarding current and planned applications of Far UV-C radiation, research priorities, and development of regulations related to Far-UV-C-based applications.

The UV Spectrum and Far UV-C

The ultraviolet spectrum is a band of electromagnetic radiation at higher energies (*i.e.*, shorter wavelengths) than visible light (see Figure 1), divided into three major categories: UV-A (315-400 nm), UV-B (280-315 nm), and UV-C (100-280 nm); vacuum-UV (VUV, 100–200 nm), is further defined as a sub-category of UV-C. While there are some differences among definitions that have been presented to define the ranges of UV radiation, for the purposes of this White Paper, we further sub-divide UV-C into germicidal UV (UVGI at 250-280 nm), Far UV-C (at 200–230 nm), and vacuum-UV (VUV, at 100–200 nm).[†]

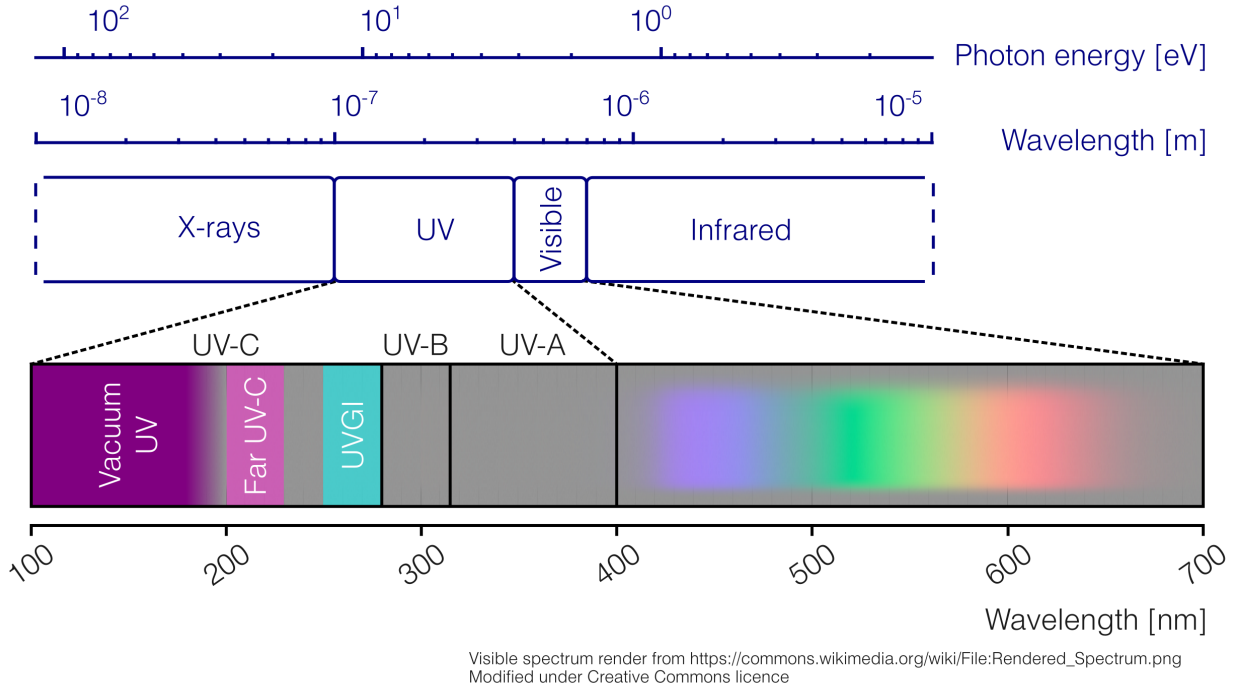

Visible spectrum render from https://commons.wikimedia.org/wiki/File:Rendered_Spectrum.png
Modified under Creative Commons licence

Figure 1. Electromagnetic spectrum and the position of ultraviolet radiation within it. Designations of the wavelength ranges that define UV-A, UV-B, UV-C are shown, along with the sub-categories of UV-C (UVGI, Far UV-C, and VUV).

[†] Note: The wavelength ranges listed above conform to the definitions provided by the International Commission on Illumination (CIE) (see http://cie.co.at/eilvterm/17-21-008). Another prominent professional organization, the International Union of Pure and Applied Chemistry (IUPAC), presents a slightly different set of wavelength ranges for these categories of UV radiation (see https://goldbook.iupac.org/terms/view/UT07492). Specifically, the IUPAC defines UV-A and UV-B in the same manner as CIE, but defines UV-C as radiation with wavelengths of 200-280 nm, while VUV is defined as radiation with wavelengths of 100-200 nm

Sources of Far UV-C Radiation

UV-C inactivation relies on the generation of UV radiation from artificial sources. The most common Far UV-C sources are barrier discharge excimer lamps,[1] first developed in the 1980s.[2] In these devices, a voltage is applied across a sealed chamber containing a rare gas-halogen mixture exciting the gas into a plasma state; the resulting excited molecular complex then undergoes an electron transition to emit quasi-monochromatic radiation. Various excimers may form in the plasma, leading to primary and secondary (weaker) emission peaks. The contributions from different electron transitions may, to an extent, be enhanced or suppressed by tuning the lamp design (*e.g.*, gas pressure and composition).[3]

Recent work has focused on krypton-chloride excimer (KrCl*) lamps. Emission spectra vary somewhat depending on the lamp design, with KrCl* lamps typically exhibiting a dominant peak at ~222 nm with full-width-half-maximum ~4 nm; in addition there are also lower wavelength emissions extending to 200 nm and below, and higher-wavelength emissions from other KrCl* and Cl_2* transitions,[1] extending to ~300 nm and above (Figure 2). These off-nominal emissions can represent up to ~15% of the total power output of a typical unfiltered KrCl* lamp, as illustrated by full emission, unfiltered spectra, shown in Figure 2.

In practical terms, the emission peak from a KrCl* lamp centered at 222 nm is well-suited to the applications that are discussed in this document. Radiation at longer wavelengths can be problematic in terms of human eye and skin exposure risks, while shorter wavelengths can be problematic due to potential ozone generation. As such, most practical applications of KrCl* should include optical filters to minimize contributions of radiation from wavelengths significantly longer or shorter than the peak centered at 222 nm (also illustrated in Figure 2). The majority of Far UV-C research involves optically-filtered KrCl* lamps.

Other gaseous lamp based technologies may also be possible for generation of Far UV-C radiation, such as metallic vapor lamps[4] or optically-filtered medium-pressure mercury lamps,[5] though their practical utility has yet to be demonstrated for UV-based air and surface disinfection applications.

Solid state emitters in the Far UV-C range have recently been demonstrated,[6] using conventional UV-C LED construction with thin layers of AlGaN to form the LED's photon-generating "active region." These devices are benefitting from recent developments in longer-wavelength UV-C LEDs,[7] though each step toward shorter wavelengths uncovers new challenges that must be overcome. At present, Far UV-C LEDs are limited to micro-Watt outputs and exhibit short lifetimes,[8] and so do not currently represent a viable technology for disinfection. It should be noted, however, that a similar set of challenges was faced, and overcome, by UV-C LEDs in the 250–280 nm range. More exotic solid-state formulations, such as hexagonal BN layers[9] and nanowire structures,[10] have been demonstrated, though these devices are not ready for commercial application. The various construction methods and compositions of these solid-state emitters lead to significant variation in peak and bandwidth characteristics, and emissions are not necessarily confined to the Far UV-C range.

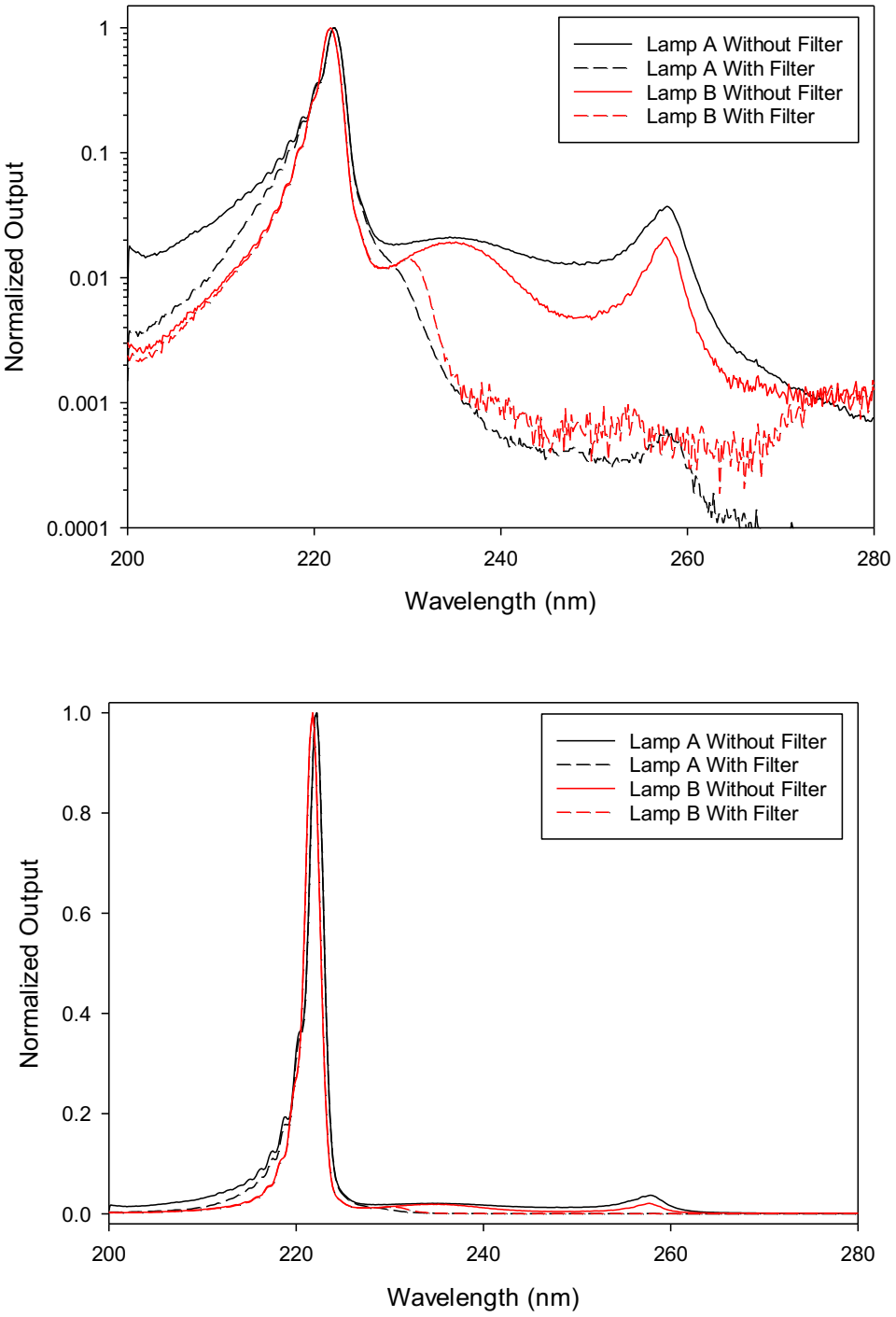

Figure 2. Emission spectra from commercially-available KrCl* lamps with and without optical filters. Normalized output presented on a $\log_{10}$ scale (top panel) and on a linear scale (bottom panel). For both lamps, the spectra were measured independently and normalized to output at the wavelength corresponding to peak output (*ca.* 222 nm).

Inactivation By UV-C/Far UV-C Radiation

How Far UV-C Works - Inactivation Mechanisms

UV inactivation is controlled by two key parameters: wavelength and total UV exposure (commonly referred to as UV dose or fluence).[11, 12] Germicidal efficacy varies with UV-C wavelength and is unique to the microbe or virus being targeted: the germicidal action spectrum describes this response. Though germicidal action spectra vary among microbial and viral species,[13] a common feature is a local peak in the 260–270 nm region, where UV-C causes nucleic acid breakdown resulting in inactivation of the pathogen (aka, disinfection). This, coupled with the ready availability of mercury vapor-based lamps led to the historic focus of conventional mercury vapor-based UVGI systems (emitting predominantly at 254 nm).

Wavelengths below 230 nm are typically highly effective for inactivation due to the absorbance of photons by both nucleic acids and proteins (see Figure 3); however these wavelengths have been less widely researched, presumably because of the difficulty in finding UV-C sources operating at this region. The absorbance of Far UV-C by nucleic acids and proteins can lead to photochemical damage to both biomolecule types, providing two pathways to inactivation of microorganisms and viruses.

While these shorter Far UV-C wavelengths are more readily absorbed by target pathogens, they can also be readily absorbed by surrounding media, resulting in reduced inactivation. For example, airborne viral pathogens are often contained within aerosol droplets, which themselves often contain relatively high concentrations of proteins. The presence of these compounds may limit penetration of Far UV-C radiation into aerosols, depending on the aerosol diameter and composition, which in turn will influence delivery of photons to the target pathogens.[14] At present, the effects of absorbance by aerosol proteins (and other constituents) are understood at a qualitative level but expected to be minimal due to the short optical pathlength; improvement of our understanding of the effects of this behavior in quantitative terms represents an area for future research.

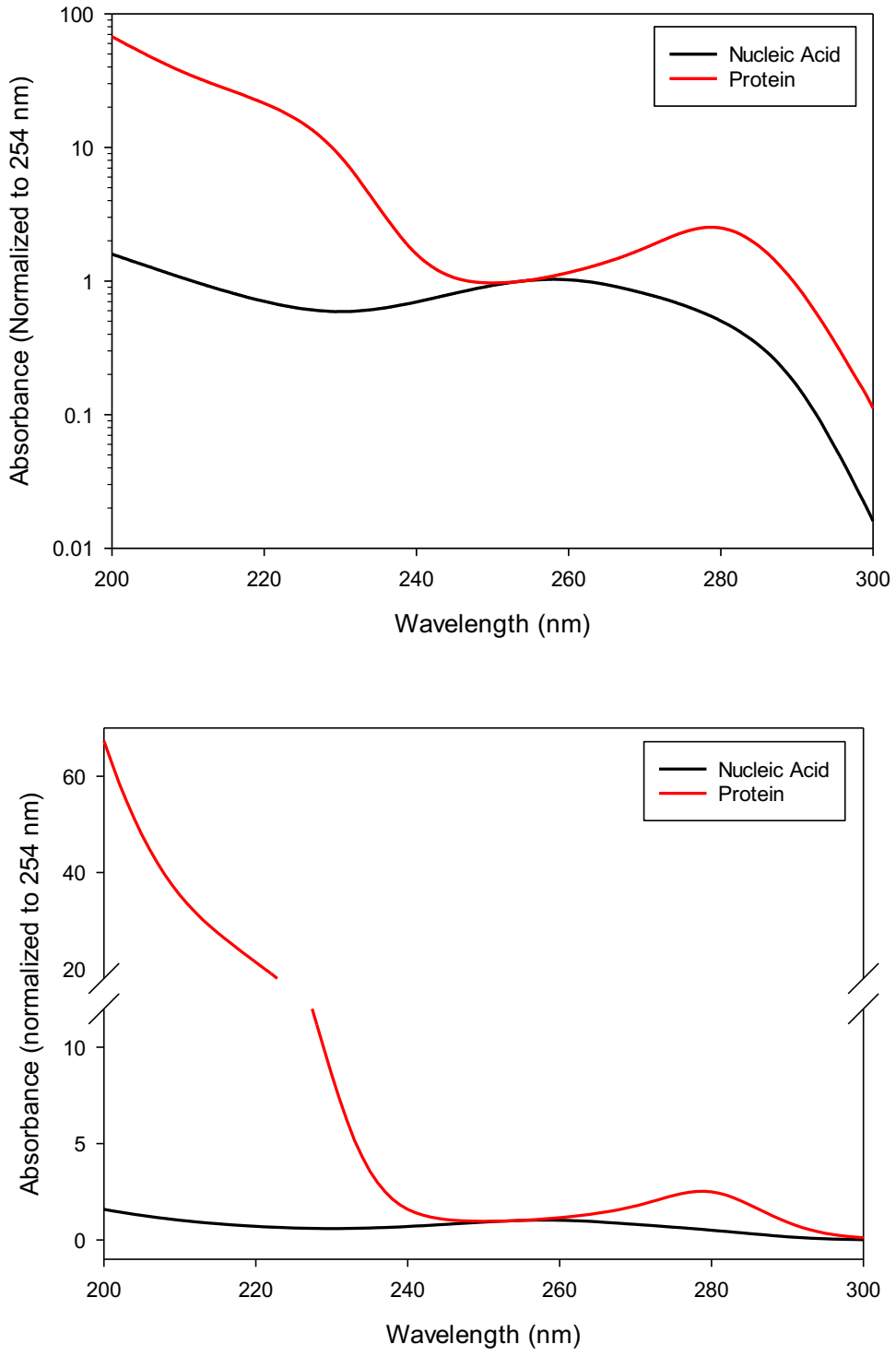

Figure 3. Normalized absorbance of nucleic acids (DNA/RNA) and the protein trypsin (in dry form); (top) $\log_{10}$-scale, (bottom) linear scale (reproduced from Setlow *et al.*[15] Voet *et al.*[16]).

How Much Far-UV-C Is Required - Inactivation Studies

The term "log inactivation" (or informally "log kill" [*sic*]) is often used to describe the effect of disinfectant exposure on a pathogen population. The formal definition of log inactivation is:

$$\boldsymbol{X\ log_{10}\ units\ of\ inactivation\ translates\ to\ \frac{N}{N_0} = 10^{-X}} \qquad (1)$$

As examples, 1 $\log_{10}$ unit of inactivation corresponds to 90% inactivation $\left(\frac{N}{N_0} = \mathbf{0.1}\right)$, 2 $\log_{10}$ units of inactivation corresponds to 99% inactivation $\left(\frac{N}{N_0} = \mathbf{0.01}\right)$, 3 $\log_{10}$ units of inactivation corresponds to 99.9% inactivation $\left(\frac{N}{N_0} = \mathbf{0.001}\right)$, and so on. This equation is the basis for the scales and the data plotted in Figures 4, 5, and 7-9.

UV-C irradiation is effective against microbial and viral pathogens in air, water, and on surfaces. Coronaviruses specifically are highly susceptible to UV-C radiation, as illustrated in Figures 4 and 5. Using data from studies conducted based on aqueous (liquid) suspensions of viruses employing accepted guidelines or best practice and methods for measuring UV dose and for assessing viral inactivation, it can be seen that this behavior holds for irradiation from a conventional 254 nm emitting lamp, as well as from sources that emit at other UV-C wavelengths, including Far UV-C.

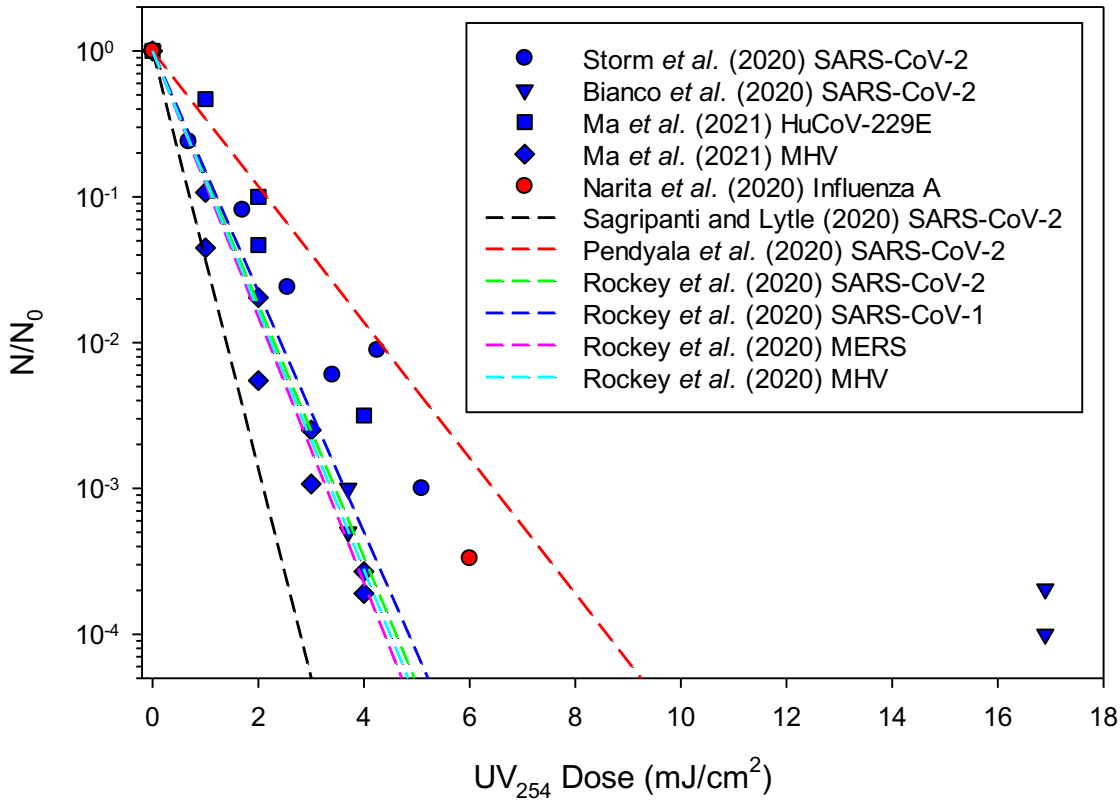

Figure 4. Measured UV_{254} dose-response behavior of common ssRNA respiratory pathogens, including numerous coronaviruses, in aqueous suspension. Measured inactivation responses of coronaviruses are indicated by blue symbols; measured inactivation of Influenza A virus is indicated by red symbols. Also included are predictions of coronavirus responses from genomic models (dashed lines).

As an example, at 254 nm, approximately 1 $\log_{10}$ reduction of coronaviruses is achieved for each 2 mJ/cm^2 delivered UV-C fluence ("dose"), as illustrated in Figure 4, above. For comparison, pathogenic viruses such as poliovirus and rotavirus require roughly 4-5 times that amount (i.e., 8-10 mJ/cm^2) for each $\log_{10}$ unit reduction.

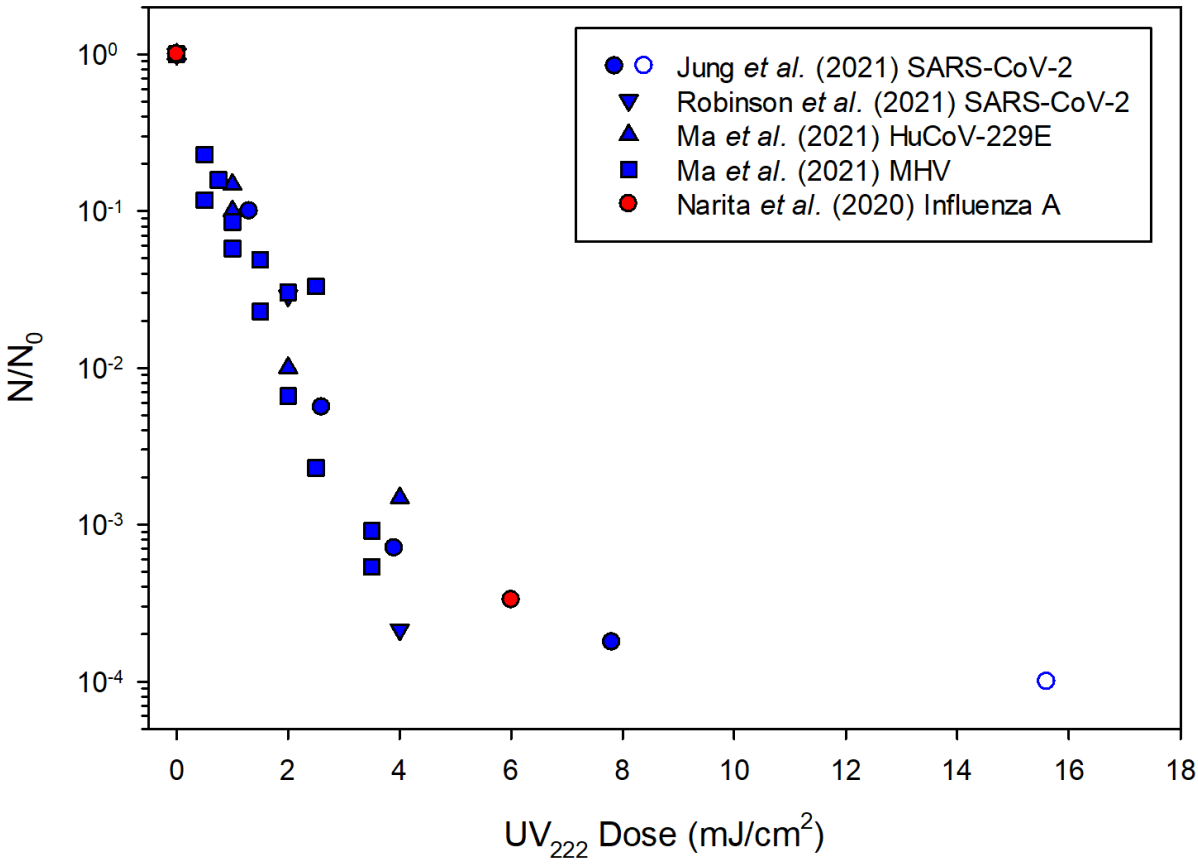

Figure 5. Measured UV_{222} dose-response behavior of common respiratory ssRNA viruses including numerous coronaviruses in aqueous suspension. Measured inactivation responses of coronaviruses are indicated by blue symbols; measured inactivation of Influenza A virus is indicated by red symbols. The open symbol represents a reported value beyond the detection limit of the viral infectivity assay.

Based on experimental data available, 222 nm UV irradiation is at least as effective as 254 nm UV irradiation for inactivation of viruses and phage viral surrogates and the data suggest that about 2 $\log_{10}$ reduction of coronaviruses is achieved for each 2 mJ/cm^2 delivered UV-C fluence, as illustrated in Figure 5, corresponding to roughly twice the rate of inactivation as observed at 254 nm. Therefore, data for 254 nm UV inactivation can conservatively represent the expected virus inactivation at 222 nm.

Genome size, measured in kilo-bases (kb) or kilo-base pairs, has been demonstrated as a key factor that governs the response of viruses to UV-C radiation.[17-20] In general, large genomes provide more targets for photochemical damage, and as such, viruses with larger genomes tend to be inactivated relatively quickly. The type of genome (either single-stranded [ss], double-stranded [ds], RNA, or DNA) can also influence the responses of viruses to UV-C exposure. For context, the coronaviruses have the largest known genomes among ss-RNA viruses; this appears to be an important contributing factor to the ease with which coronaviruses are inactivated by UV-C exposure. Viruses with ds genomes are often relatively resistant to UV-C exposure because the complementary nucleic acid strand can facilitate repair. The presence of a viral envelope can influence the susceptibility of viruses to exposure to some physical agents, such has heat or shear forces. However, it is not clear that the presence of a viral envelope influences the responses of

viruses to UV-C exposure. A summary of the genetic properties of the viruses and bacteriophage reported herein is presented in Table 1.

Table 1. Summary of genetic properties of human viruses and bacteriophage described herein. Sequencing information can be found in https://www.ncbi.nlm.nih.gov/, using NCBI accession number.

Virus	Genome Type	Enveloped or non-enveloped	Genome size (kilobases or kilobase pairs)	NCBI accession
SARS-CoV-2	ssRNA	Enveloped	29.8 kb	MN908947
SARS-CoV-1	ssRNA	Enveloped	29.7 kb	NC_004718
MERS	ssRNA	Enveloped	30.1 kb	NC_019843.3
MHV	ssRNA	Enveloped	31.3 kb	AY700211
HuCoV-229E	ssRNA	Enveloped	27.3 kb	NC_002645
HuCoV-OC43	ssRNA	Enveloped	30.7 kb	NC_006213
Influenza A (H1N1)	segmented ssRNA	Enveloped	13.5 kb	NC_002016-002023
Adenovirus (Type 2)	dsDNA	Non-enveloped	35.9 kb	AC_000007
Φ6 Bacteriophage	segmented dsRNA	Enveloped	13.4 kb	NC_003714-003716
T1 Bacteriophage	dsDNA	Non-enveloped	48.8 kb	NC_005833
T1UV Bacteriophage	dsDNA	Non-enveloped	(assumed similar to T1)	n/a
Qβ Bacteriophage	ssRNA	Non-enveloped	4.2 kb	NC_001890
MS2 Bacteriophage	ssRNA	Non-enveloped	3.6 kb	NC_001417

Inactivation models based on genomic properties of viruses have recently been developed for 254 nm UV irradiation.[18-20] These models yield predictions that are similar to reported measurements of viral inactivation at 254 nm; moreover, the predictions of these models are consistent with each other. Currently, no models exist to characterize UV dose-response behavior for 222 nm UV irradiation, likely due to the additional importance of protein damage in Far UV-C inactivation mechanisms[21] that genomic-based models cannot represent. The enhanced inactivation of viruses at Far UV-C wavelengths, compared to UV 254 nm, such as represented by studies on respiratory adenoviruses illustrated in Figure 6,[22, 23] has been shown to be due to protein damage.[21]

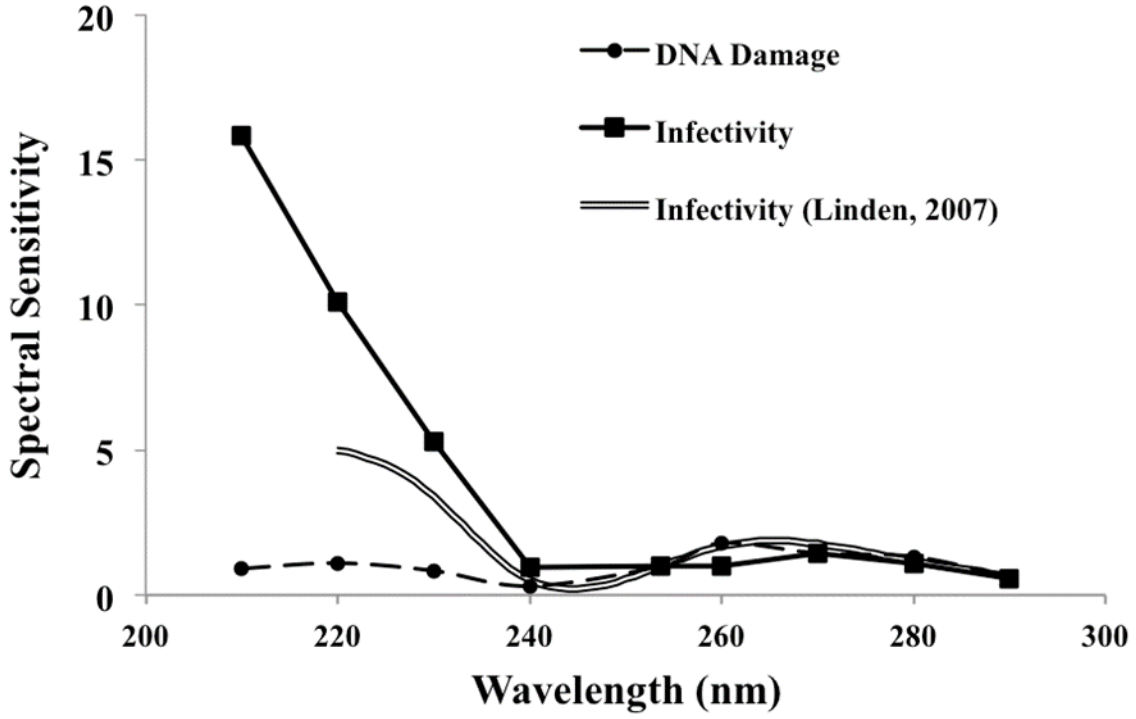

Figure 6. Spectral sensitivity of adenovirus 2 as measured by infectivity, compared to nucleic acid (DNA) damage, for wavelengths between 210 and 290 nm.[22]

Compared to UV inactivation of viruses in aqueous media, the inactivation of coronaviruses on surfaces or in aerosols appears to be slightly more effective, with greater than 1 $\log_{10}$ reduction achieved for each 2 mJ/cm^2 delivered UV dose (see Figure 7). Based on these and other available UV inactivation data, inactivation of viruses suspended in water or other aqueous media appears to provide a conservative estimate of the inactivation response that can be achieved on surfaces or in aerosols.

These data suggest that the inactivation of viruses using either 222 nm or 254 nm on surfaces or in aerosols is expected to be greater than in aqueous suspension. However, inactivation of pathogens (including viruses) in aerosols and on surfaces by exposure to UV-C radiation is also complicated by the effects of absorption by the surrounding media. As a result, quantification of UV-C dose delivery to (viral) pathogens in aerosols and on surfaces can be difficult. Extrapolation of these initial findings to other surface types and conditions is currently a subject of on-going research.

Properly designed experiments to measure UV-C dose-response behavior involve the use of a UV-C exposure device that delivers a controllable, quantifiable dose to a viral population. By conducting these exposures over a range of relevant UV-C doses, with corresponding culture-based measurements of virus or microbe inactivation, it is possible to quantify UV-C dose-response behavior. For aqueous suspensions of viruses or microbes, these experiments often involve a (pseudo) collimated beam,[24] for which well-defined, standardized methods have been established.[25] For airborne and surface-associated viruses, no such standard currently exists, although several competing guidelines and laboratory devices have been developed to approach the objectives described above.[26]

A complicating factor in the translation of UV-C dose-response behavior to practical applications, such as disinfection of air or surfaces, is the fact that the target population of pathogens is almost certain to receive

a distribution of doses, *i.e*., some pathogens may receive high doses, and some may receive low doses. Principles of process engineering dictate that the low dose population will control disinfection efficacy, often described by $\log_{10}$ reduction of the target pathogen population. The dose distribution delivered by an air disinfection system will be influenced by power, placement, and distribution of UV-C sources, as well as air circulation for air disinfection and surface characteristics (*e.g*., shadowing, gaps, and crevices) for surface disinfection. For UV-C systems used for disinfection of water, numerical methods involving integrated applications of computational fluid dynamics and fluence rate field modeling have become the industry standard for system design, as well as for simulations of the UV-C dose distribution and process performance.[27-35] It is likely that simulations and design of UV-C disinfection systems for air and surfaces will benefit from similar modeling approaches and work in this area has begun.[36] These numerical models can be used to simulate dynamic and steady-state behavior of UV-C disinfection systems, including those used to disinfect air and surfaces. The models themselves require validation based on physical measurements. Research in this area is likely to continue to evolve as interest and demand for UV-based disinfection systems grows.

Beyond the numerical models, it is also important that empirical (experiment-based) methods emerge for testing and validation of UV-C systems that are used to disinfect air and surfaces. Here again, there is a considerable knowledge base that can be drawn on from UV-C systems that have been applied for disinfection of water. Well-defined protocols for testing and validation of these systems have been established in the United States[37, 38] and in western Europe.[39-43] In general, these testing and validation protocols are based on the use of surrogate challenge microbes or viruses to quantify disinfection efficacy. Given the history and success of these applications, and the fact that they are based on measurements of inactivation of non-pathogenic challenge agents that are well-understood within the engineering and regulatory communities, it is likely that testing and validation protocols for UV disinfection systems that are used for air and water will adopt a similar strategy. However, research related to the application of UV-C radiation for disinfection of air and surfaces is not as mature as for water-based applications, and details of these methods still need to be refined.

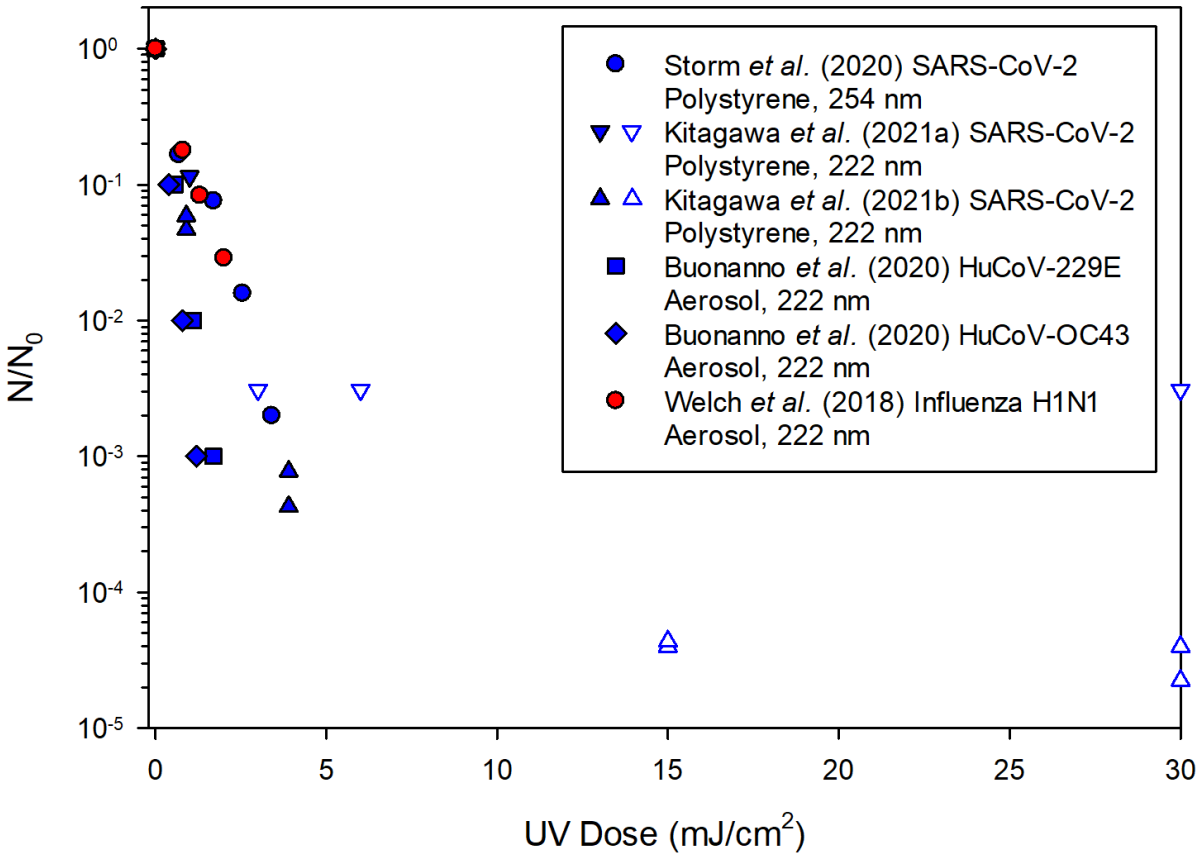

Figure 7. UV inactivation of ssRNA respiratory viruses on surfaces and in aerosols at 222 nm and 254 nm. Measured inactivation responses of coronaviruses are indicated by blue symbols; measured inactivation of Influenza H1N1 virus is indicated by red symbols. The open symbols represent reported values beyond the detection limit of the viral infectivity assay.

Surrogates for UV Inactivation of Respiratory Viruses

UV inactivation of coronaviruses can be represented by inactivation of certain phage surrogates at both 254 and 222 nm as illustrated in Figures 8 and 9, respectively. A good surrogate will be non-pathogenic to humans, easy to culture and assay, and be no more sensitive to UV exposure than the target pathogen at the wavelength(s) emitted by the UV source of interest. Identification of surrogates for SARS-CoV-2 (and other airborne viral pathogens) offers the potential to quantify or validate the performance of UV-based mitigation measures.

At 254 nm, the rate of inactivation of coronaviruses can be represented by T1UV phage, T1 phage, or more conservatively by Qβ phage. For 222 nm irradiation, the rate of inactivation of coronaviruses can be represented by T1UV or Φ6 phage, or more conservatively by Qβ phage. MS2 phage could be employed as a conservative surrogate for both 254 nm and 222 nm radiation, though with varying sensitivity at each (data not shown because they are inconsistent with the vertical axis scales in Figures 8 and 9). This difference in suitability of acceptable surrogates could have a meaningful impact on future validation

protocols for these technologies: a one-size-fits-all approach to UV-C disinfection is not likely to be effective across the broad range of possible applications.

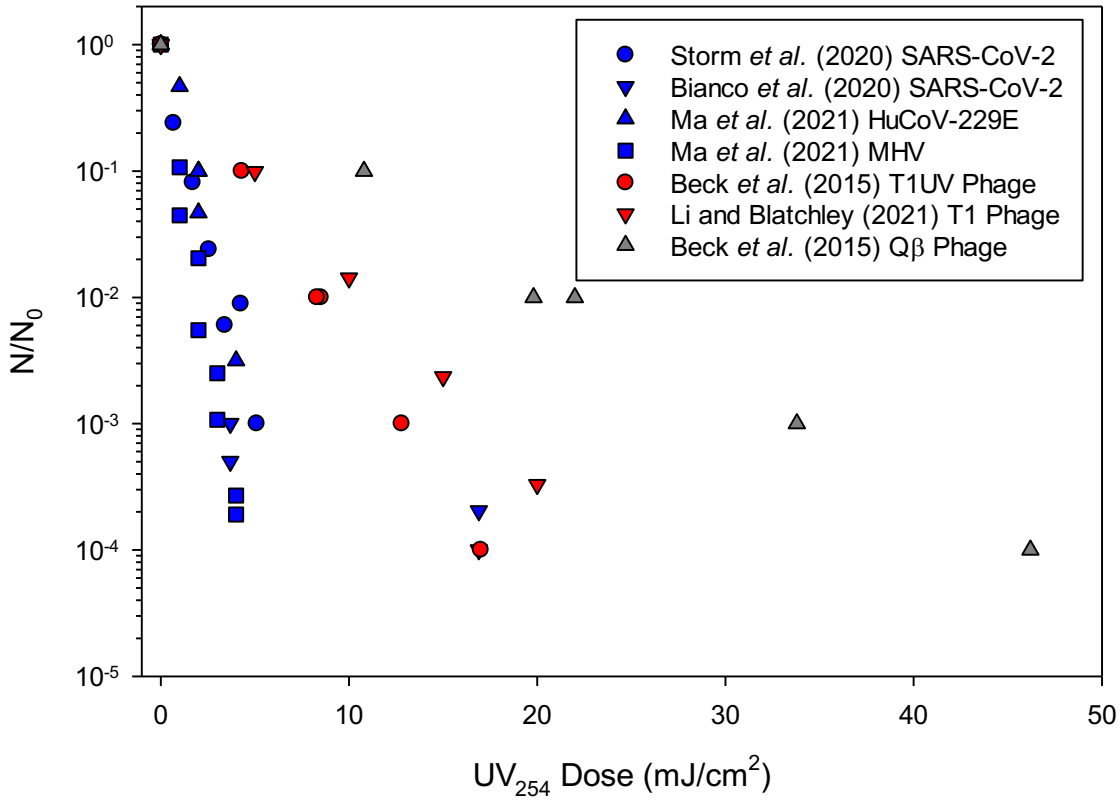

Figure 8. UV_{254} dose-response behavior of coronaviruses and phage that could serve as (conservative) surrogates. Measured inactivation responses of coronaviruses are indicated by blue symbols; measured inactivation responses of potential phage surrogates are indicated by red symbols; measured inactivation responses of conservative phage surrogates are indicated by charcoal gray symbols.

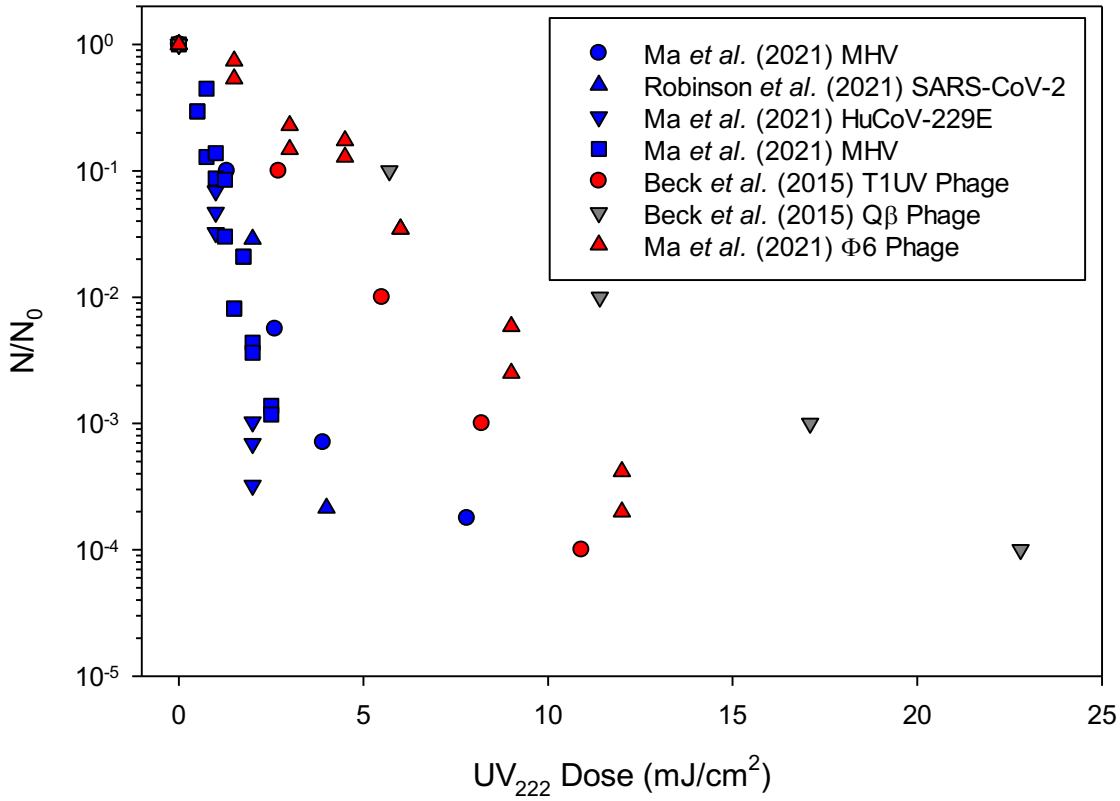

Figure 9. UV_{222} dose-response behavior of coronaviruses and phage that could serve as (conservative) surrogates. Measured inactivation responses of coronaviruses are indicated by blue symbols; measured inactivation responses of potential phage surrogates are indicated by red symbols; measured inactivation responses of conservative phage surrogates are indicated by charcoal gray symbols.

Safety Aspects of Human Exposure to Far UV-C Radiation

Multiple recent studies of health effects from Far UV-C exposures of the eye and skin indicate that the wavelengths below about 230 nm are substantially safer than longer UV-C wavelengths.[44-55] These experimental observations are consistent with biophysical considerations regarding the much shorter penetration depth of Far UV-C radiation as compared with longer wavelength UV-C radiation. The biophysical background here is that UV-C radiation at wavelengths less than about 230 nm is strongly absorbed by all proteins (particularly through the peptide bond) and by other biomolecules,[45, 56, 57] and so its ability to penetrate living tissue is quite limited. This phenomenon is quantified by wavelength-dependent measurements shown in Figure 10 (see also information in Figure 3). These considerations and experimental results have led to proposals to modify safety guidelines for human exposure in the Far UV-C spectral region, including for whole-room exposure in occupied settings (see below).[58-60]

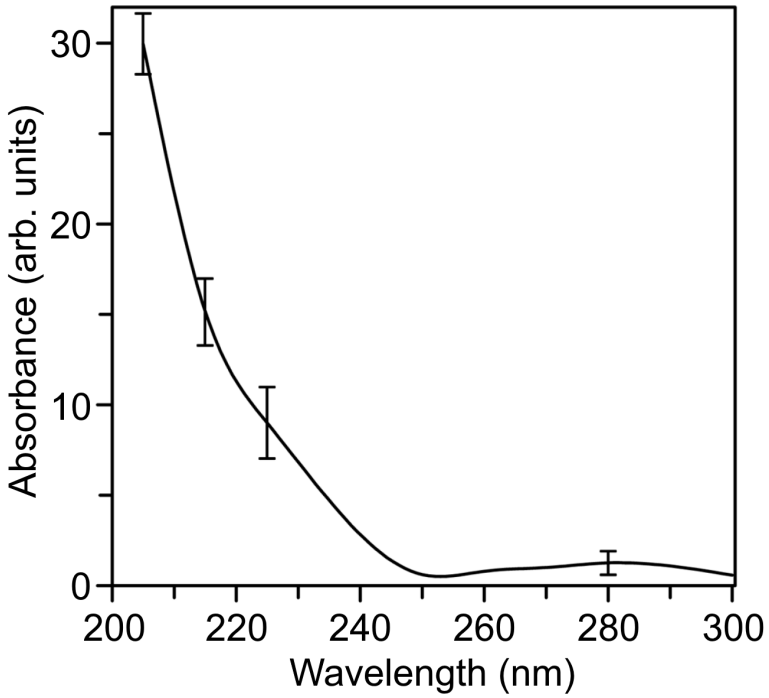

Figure 10. Measured wavelength-dependent UV absorbance, averaged over measurements for eight common proteins. From Ref. [45]

Skin

A significant concern about the safe use of UV-C in germicidal applications has long been the potential for promotion of skin cancer.[59, 61, 62] However, past reviews of the photocarcinogenesis risks focused only on 254 nm and longer UV-B and UV-A wavelengths.[63] Epidemiological studies of skin cancer clearly showed the causal factor of ambient solar radiation to be primarily attributable to the UV-B component.[64] To date, there have been no human epidemiological studies done to study skin cancer resulting solely from UV-C exposure, as this has not been a concern because so few people have been exposed. Even so, it is clear that our outermost layer of skin (*i.e*., the human stratum corneum) strongly attenuates UV-C radiation such that very little UV-C radiation reaches the germinative, basal layer of the epidermis, where the DNA would have to be altered to potentially initiate skin cancer.[49, 50, 62, 63] For Far UV-C radiation, which is more strongly attenuated in the stratum corneum than longer UV-C wavelengths or UV-B, the biophysical situation is even clearer, in that very little Far UV-C radiation reaches even the superficial layers of the epidermis, and essentially none reaches the deeper basal layer, negating Far UV-C as a cancer risk (see Figure 11).

Additionally, there have been a number of recent experimental safety studies of Far UV-C radiation in human skin and hairless mouse skin, both *in vitro* and *in vivo.* Of the ten peer-reviewed published studies, nine have shown no measurable negative impacts,[44, 46, 48-54] despite including much larger doses than would be permitted in a human exposure scenario; the one published study[55] that did show evidence of skin erythema used an unfiltered Far-UVC excimer lamp, *i.e*. with a significant component of UV-C radiation at wavelengths >230 nm; this 2015 study was essentially repeated in 2020 by Fukui *et al.*[48] using optically-filtered 222 nm radiation (*i.e*., without the >230nm components) at similar and higher doses, and no evidence of erythema or any skin safety risk was observed.

These *in-vivo* human skin results are consistent with the recent studies by Buonanno *et al*.[54] who applied a well-established *ex-vivo* human skin model (EpiDerm), where no significant increased yields of pre-

mutagenic cyclobutane-pyrimidine-dimer (CPD) DNA lesions were seen after exposure to 125 mJ/cm^2 of unfiltered Far-UVC radiation, and a slight increase at 500 mJ/cm^2 was seen. In turn, these results are consistent with the results from Yamano *et al.*[52] who conducted a study with hairless mice; they exposed two genotypes of hairless mice that are highly susceptible to carcinogenesis to a Far-UV-C dose of 500 mJ/cm^2 and reported a faint detection of CPDs, but only in the uppermost cells of the epidermis, a finding recently duplicated in *in-vivo* human skin studies.[53] These most superficial, outer-most cells of the epidermis are at the end of their lifetime, about to become the dead cells that comprise the outermost skin layer – the stratum corneum. Consistent with these observations, Yamano *et al.*[52] reported no evidence for Far-UV-C-induced skin cancer in their study with skin-cancer prone mice. The demonstration of little or no skin damage at these exposures (being above those typically required for disinfection) supports the application of germicidal Far UV-C technology in occupied spaces.

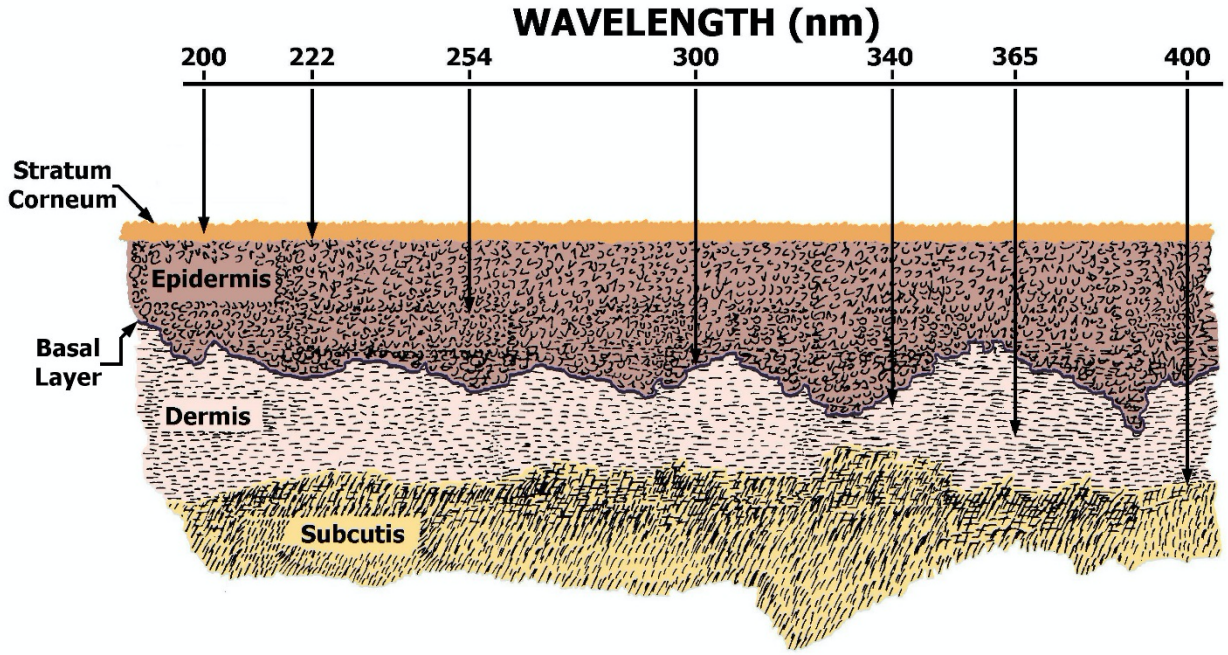

Figure 11. Penetration of UV wavelengths into human skin; arrows represent an estimate of 90% absorption depth. UV-C wavelengths at 222 nm do not appear to penetrate the stratum corneum; whereas, 254 nm does penetrate into upper epidermis. UV-B wavelengths, such as 300 nm, do penetrate to the critically important germinative (basal) layer of the epidermis and have sufficient energy to mutate DNA. UV-A wavelengths at 340 nm, 360 nm, and 400 nm penetrate well into the dermis, but the lower photon energies are far less damaging than 300 nm. [Figure courtesy of DH Sliney].

Eye

There have been quite limited studies of the effects of ocular exposures to Far UV-C wavelengths. Kaidzu *et al*. [47, 65] assessed threshold photokeratitis in a rat eye model. They conducted assessments at 24 hrs post exposure using slit-lamp bio-microscopy, staining, and surface mapping. They reported exposure thresholds at four UV-C wavelengths (nominally 207 nm, 222 nm, 235 nm, and 254 nm) as well as one UV-B wavelength (311 nm); the measured thresholds for a detectable effect on the cornea at 207 nm and 222 nm were above 5,000 mJ/cm^2 and 15,000 mJ/cm^2 respectively, which are far above the current safety guidelines. Kaidzu *et al.* [47, 65] also undertook a histological assessment of the cornea using CPDs as a marker for DNA damage, which were analyzed for each wavelength and as a function of exposure dose. The depth of observed CPDs varied with wavelength; for the Far UV-C 207 nm and 222 nm exposures, the CPD biomarker was only observed in the upper superficial cells of the corneal epithelium, cells which are

sloughed off in a few days in the normal corneal epithelial life cycle. Analogous to the skin, the germinative cells of the cornea are located in the limbus, at the border between the cornea and conjunctiva, and are thus protected from Far UV-C radiation by several cell layers (see Figure 12). By contrast, in their corresponding studies with 254 nm and 313 nm exposures, CPDs were observed in all layers of the cornea including the corneal endothelium.

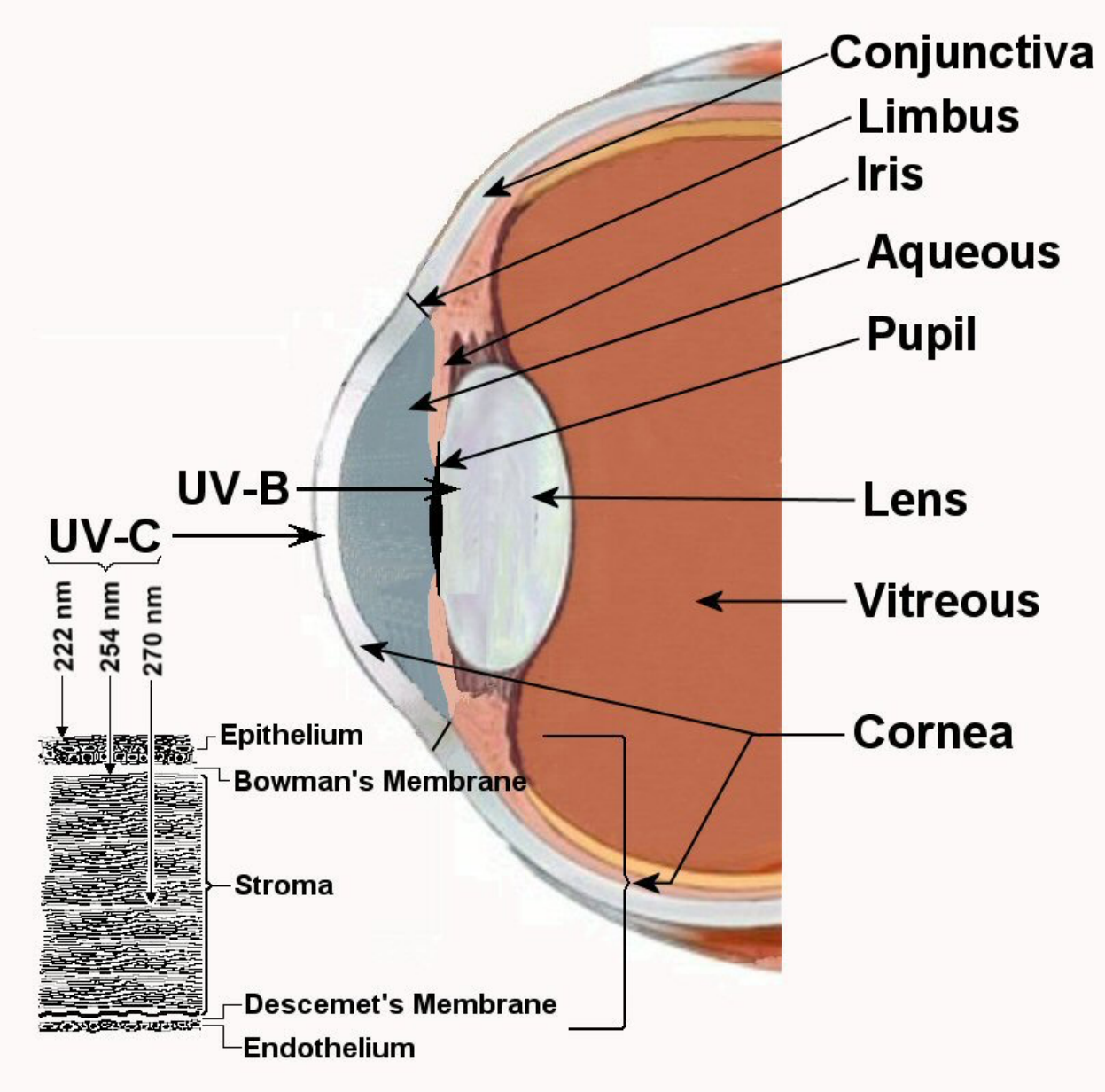

Figure 12. Penetration of UV wavelengths into the human eye. UV-C wavelengths at 222 nm hardly penetrate to the corneal epithelium; whereas, 254 nm does penetrate well into the epithelium and into the stroma. There is some evidence of penetration even to the endothelium. UV-B wavelengths, such as 300 nm do penetrate to the lens, and oblique rays to the critically important germinative layer of the lens behind the iris and have sufficient energy to mutate DNA. UV-A wavelengths are strongly absorbed by fluorophores in the lens and protect the retina. [Figure courtesy of DH Sliney].

The corneal injury thresholds reported by Kaidzu *et al.*[47, 65] for Far-UVC radiation are significantly higher than those reported by Pitts.[66] A likely explanation is that Pitts used wide-bandwidth arc-monochromator exposures centered at 220 nm, 240 nm, and 250 nm. The bandwidths were sufficiently large (10 nm full-width, half-maximum, FWHM) that the derived action spectrum was severely flattened, as also occurred in the 310-nm region.[67] Since the Pitts data were used in development of the current UV exposure limits,[60, 68] these limits are overly-conservative, as discussed below.

Exposure Limit Guidelines

The guidelines for human exposure to UV-C radiation currently are identical worldwide. The best-known limits are from the American Conference of Governmental Industrial Hygienists (ACGIH) and the International Commission on Non-Ionizing Radiation Protection (ICNIRP); these published limits have remained largely unchanged for at least 3 decades.[58, 69]. The spectral weighting function, S(λ), was based upon corneal and skin injury thresholds available in the 1970s, and fortunately there were thresholds available in the UV-B that were from monochromatic thresholds.[60] Figure 13 provides a graphical summary of the current guidance values of S(λ) across the UV spectrum. Figure 14 illustrates the corresponding 8-hr exposure limits.

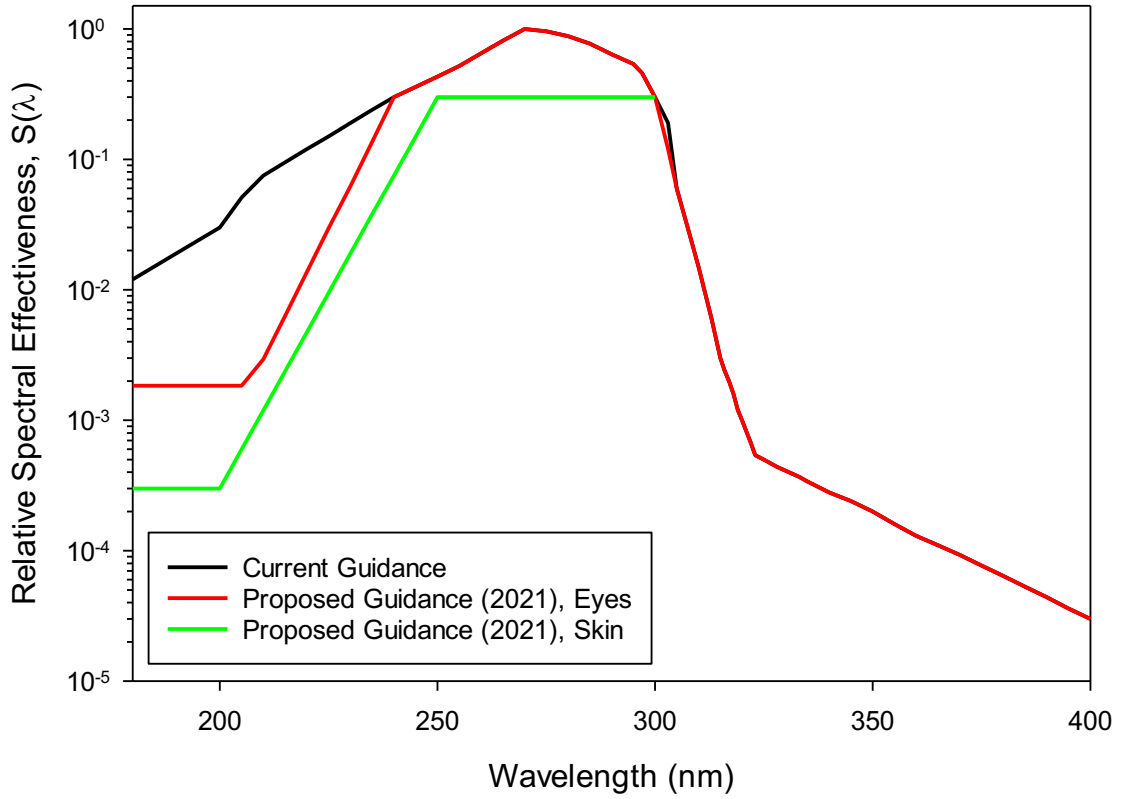

Figure 13. Comparison of current and proposed guidance for relative spectral effectiveness, *S(λ),* as a function of wavelength. Proposed guidance values were presented by ACGIH. Proposed values for eye exposure are protective of skin; proposed values for skin are presented for circumstances where human eyes are protected from exposure.

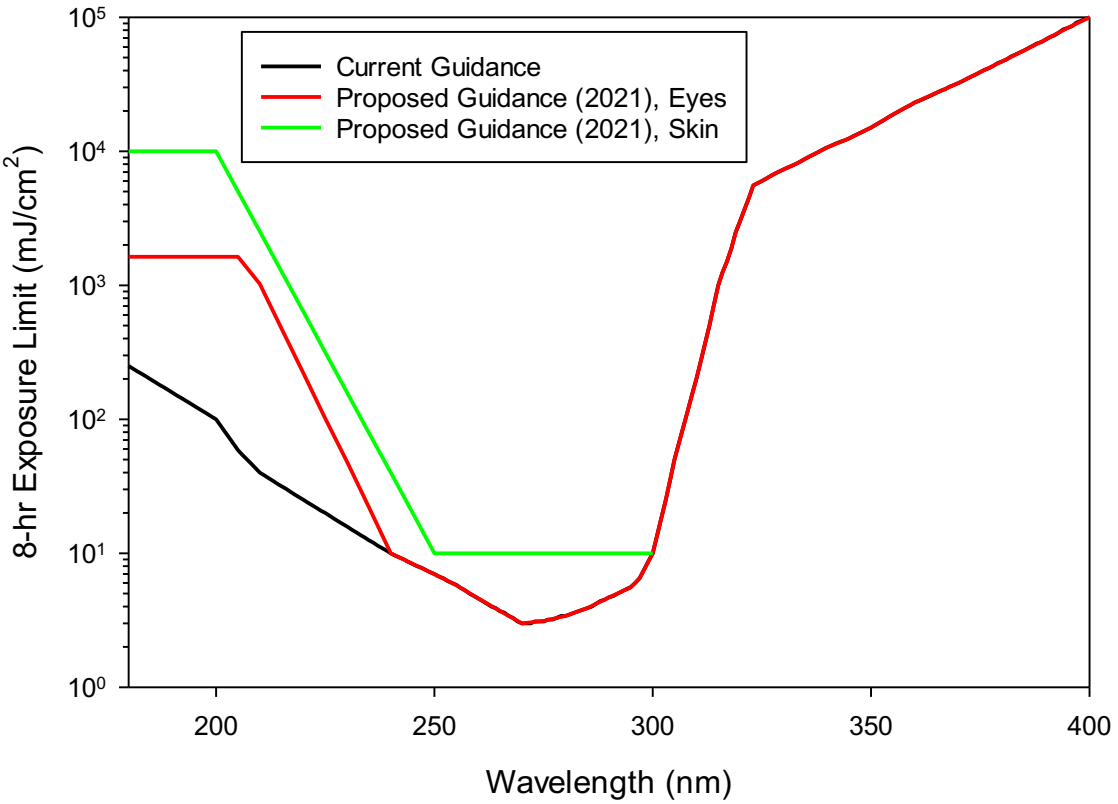

Figure 14. Comparison of 8-hr exposure limits for UV-C radiation, based on relative spectral effectiveness values illustrated in Figure 13.

In 2020 the ACGIH issued a "Notice of Intended Change" of the UV Threshold Limit Values (TLVs), and these proposals incorporated for the first time a separation of limits for the eye and skin at wavelengths below 300 nm and an increase in current limits for the eye at wavelengths below 250 nm.[58] The proposed values of S(λ) for skin and eye exposure are also included in Figure 13 to allow comparison with the existing values. Exposure limits based on the proposed values of S(λ) for skin and eye exposure are illustrated in Figure 14. The proposed daily (based on an 8-hour exposure period per day), time-weighted exposure limits at 222 nm would rise from 23 mJ/cm^2 (for both skin and eyes) to 161 mJ/cm^2 for the eye and 479 mJ/cm^2 for the skin. The skin exposure limits are perhaps still rather more conservative than might be justified by the data described above.

Risks for Sensitive Individuals for Exposure to Far UV-C Radiation

Risk estimates of necessity refer to populations, though the Exposure Limit Guidelines discussed above are designed to be sufficiently conservative as to account for a reasonable distribution of sensitivities. Here we consider the tissue subcategories of individuals who might potentially be systematically more sensitive than average to the effects of Far UV-C radiation, such as those with sensitive or photosensitive skin, or with dry eye. Given that the increased skin safety associated with Far UV-C exposure derives largely from the stratum corneum thickness (SCT), then it is relevant that SCT is not significantly different between individuals who do or do not have "sensitive skin."[70] Likewise, SCT is not statistically significantly different between individuals who have skin cancers vs. healthy individuals.[71] Also the SCT is generally independent of age, sex, and race [72]. Correspondingly for the eye, in a study of tear-layer thickness in dry-

eye patients, there was no significant difference in the muco-aqueous tear layer thickness or the lipid tear layer thickness in healthy *vs*. mild-moderate *vs*. severe dry-eye patients.[73] Therefore, the available data do not provide evidence that there are significant subgroups of individuals who, by virtue of age, sex, race, health conditions, or genetics, are systematically more sensitive than average to the effects of far UV-C radiation.

Ozone Generation by Far UV-C Lamps

Another safety-related concern connected to Far UV-C-based applications is the potential to generate ozone. The primary focus of this section is on photochemical formation (and decomposition) of ozone; however, it should be noted that ozone may also be formed as a result of corona discharges, which are associated with some Far UV-C sources. Moreover, the accumulation of ozone in ambient air will be governed not only by reactions that lead to formation and decay of ozone, but also air circulation and mixing in the vicinity of the Far UV-C source.

Ozone Exposure Limits

Ozone has been shown to affect the respiratory system as well as the cardiovascular and central nervous systems. Exposure limits for gas-phase ozone have been established by many governmental and non-governmental organizations that have responsibilities to ensure public health. Table 2 provides a summary of exposure limits for O_3 that have been established by several of these organizations. In general, these limits call for gas-phase O_3 concentration to be maintained less than 0.05-0.1 ppm_v.

Table 2. Summary of regulatory and guideline exposure limits for gas-phase O_3.

Agency or Organization	O_3 Limit Name or Acronym	O_3 Exposure Limit ppm_v $\left(\frac{mg}{m^3}\right)$	Comments
NIOSH/OSHA[74]	TWA	0.1 $(\mathbf{0.2})$	Time-weighted average (TWA) for up to a 10-hr work day during a 40-hr work week
	ST	0.3 $(\mathbf{0.6})$	Short-term TWA
EPA[75]	NAAQS	0.070 $(\mathbf{0.14})$	Primary and secondary NAAQS; annual 4th-highest daily maximum 8-hour concentration, averaged over 3 years
WHO[76]	Guideline	0.1 $(\mathbf{0.2})$	8-hour mean exposure concentration
ACGIH	Guideline	0.05 $(\mathbf{0.1})$	Heavy work
		0.10 $(\mathbf{0.2})$	Moderate work

Reactions Responsible for Ozone Formation and Decay from Far UV-C Sources

Photochemical formation and destruction of ozone in the gas phase have been investigated extensively, largely because of the roles played by ozone in tropospheric and stratospheric chemistry, as well as with the use of vacuum UV (VUV) sources as ozone generators. Ozone $(\boldsymbol{O_3})$ is generated by short wavelength UV radiation $(\boldsymbol{\lambda \lesssim 242\ nm})$ or in electrical discharges (corona) when molecular oxygen $(\boldsymbol{O_2})$ is present. Ozone can also be generated photochemically by a combination of ozone precursors (*e.g.*, nitrogen oxides and hydrocarbons) at longer wavelengths UV $(\boldsymbol{290\ nm \lesssim \lambda \lesssim 400\ nm})$, but this mechanism of ozone formation is unlikely to contribute significantly to ozone generation by Far UV-C sources.

Much of our current understanding of the potential for ozone formation from Far UV-C sources is based on studies of ozone formation and destruction in the stratosphere, which are initiated by photochemical reactions. The basic reactions that are responsible for photochemically-initiated formation and decomposition of ozone were first proposed by Sydney Chapman in 1930. The "Chapman Cycle" comprises the following set of reactions:[77, 78]

$$\boldsymbol{O_2 + h\nu \rightarrow O + O} \quad (2)$$

$$\boldsymbol{O + O_2 + M \rightarrow O_3 + M} \quad (3)$$

$$\boldsymbol{O_3 + h\nu \rightarrow O + O_2} \quad (4)$$

$$\boldsymbol{O + O_3 \rightarrow O_2 + O_2} \quad (5)$$

$$\boldsymbol{O + O + M \rightarrow O_2 + M} \quad (6)$$

Reactions 2 and 4 in this sequence are both photochemical. The rates of these reactions are governed by the rate at which UV photons in the relevant wavelength range are absorbed by the reactant molecules. In the case of reaction 2, the reactant is molecular oxygen (O_2), while for reaction 4 the reactant is ozone (O_3).

Absorption cross-sections ($\boldsymbol{\sigma}$) indicate the ability of gases to absorb radiation as a function of wavelength.[‡] Figure 15 illustrates the absorption cross-sections (absorption spectrum) for gas-phase O_2 for wavelengths that include vacuum UV (VUV) and UV-C. Absorption starts to become quantifiable at wavelengths less than about 242 nm, which represents the practical upper limit of the wavelength range that initiates reaction 2. Within the range of wavelengths that are relevant to applications that involve UV-C and VUV, the absorption cross-sections of O_2 are characterized by the Herzberg continuum, which represents a regular, smooth increase of absorption as wavelength decreases from roughly 240 nm down to 200 nm. For wavelengths from roughly 200 nm down to 175 nm, a banded structure known as the Schumann-Runge bands becomes evident; this structure is attributable to promotion of the O_2 molecule from a ground state to excited state transitions.[79] Note that the vertical axis in Figure 15 is presented on a $\log_{10}$ scale; therefore, absorption by O_2 in the Schumann-Runge bands is several orders of magnitude more efficient than in the Herzberg continuum.

[‡] In atmospheric chemistry, the most common unit of concentration is molecules/cm^3. As in other applications of the Beer-Lambert law, a term must be included to describe the probability of photon absorption (at a given wavelength). The absorption cross-section is that term in atmospheric chemistry. Note that the common units for the absorption cross-section (cm^2/molecule) are dimensionally-consistent with those of the molar absorption coefficient (ε), with common units of L/mole·cm, that is often used in applications of the Beer-Lambert law involving liquids,

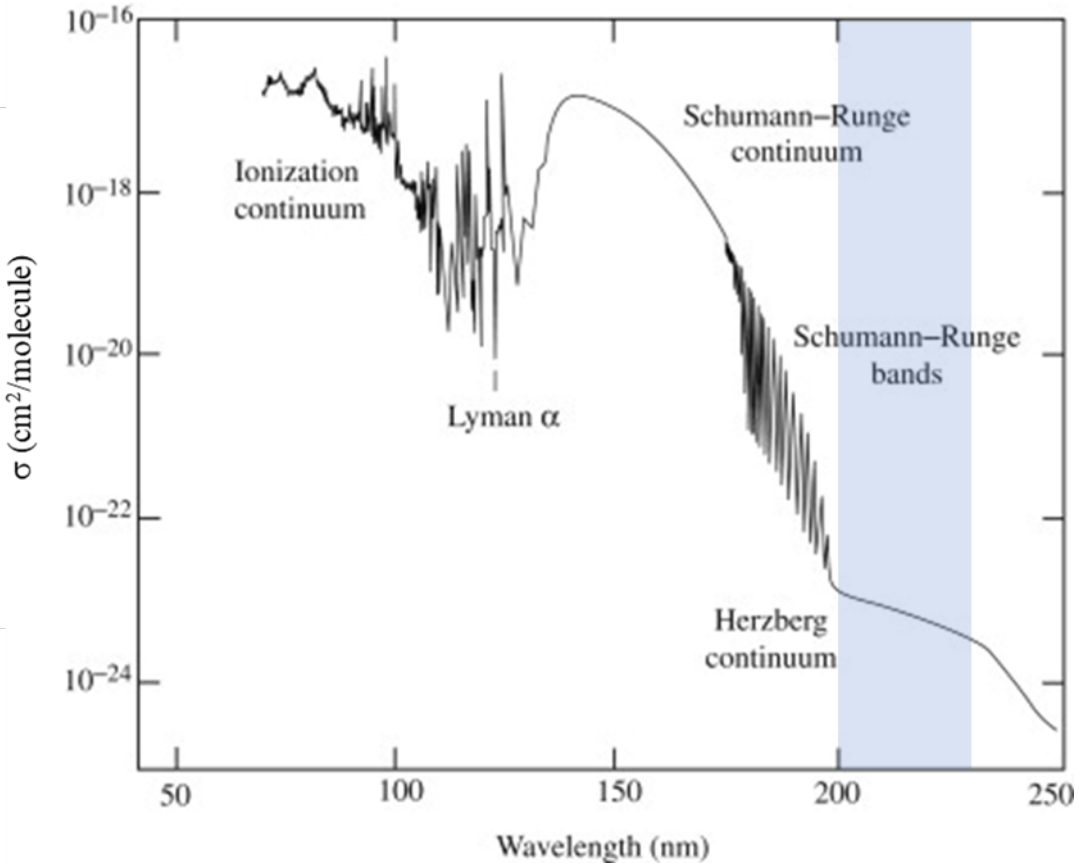

Figure 15. Absorption cross sections for molecular oxygen (O_2) for wavelengths that comprise the VUV and UV-C ranges. Image modified from *Encyclopedia of Atmospheric Sciences*.[80] The shaded blue area indicates the Far UV-C range.

Ozone is also photoactive. Wavelengths of radiation less than about 320 nm are sufficiently energetic to initiate reaction 4. As with any photochemical reaction, the absorption behavior of the reactant (in this case O_3) will play a key role in governing the kinetics of the reaction. Figure 16 illustrates recommended values of the absorption cross-sections (absorption spectrum) for O_3 for temperatures between 293-298 K (20-25°C, or nominally room temperature).

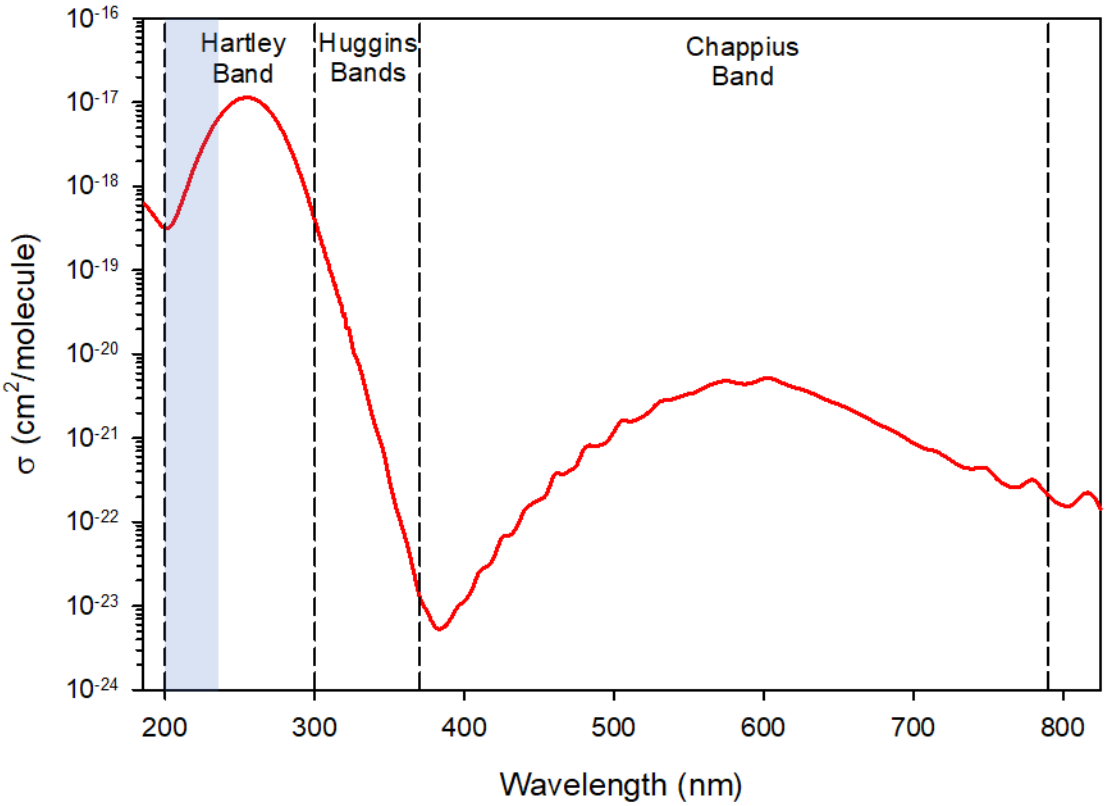

Figure 16. Recommended absorption cross-sections (σ) for O_3 for temperature in the range 293-298 K. Data from: *Chemical Kinetics and Photochemical Data for Use in Stratospheric Modeling, Evaluation Number 19*, JPL.[81] The shaded blue area indicates the Far UV-C range.

Generation of ozone will depend on balance between the rates of ozone formation and decay. Since both processes are initiated photochemically and the rates of these reactions are directly influenced by absorption of UV radiation, it is useful to compare the absorption spectra of the two reactants, O_2 and O_3. Figure 17 provides this comparison for wavelengths of radiation that are relevant to most UV-C systems where ozone may be generated, including systems that involve Far UV-C sources of radiation. The data presented in Figure 17 indicate that ozone is a much stronger absorber of UV-C radiation than molecular oxygen on a per-molecule basis; however, the concentration of O_2 is likely to be many orders of magnitude larger than the concentration of O_3. Consequently, the rate of reaction 2 is generally faster than the rate of reaction 4 with Far UV-C or VUV sources. For example, for a system operating with an air mixture at a total pressure of 1.0 atm with a temperature of 20°C and O_3 present near the regulatory limit for O_3 (0.1 ppm_v), with the ambient air being exposed to radiation at 222 nm (the peak wavelength from a KrCl* lamp), reaction 2 will proceed roughly 4.3 times faster than reaction 4. In a room where (essentially) no ozone is present (*i.e.*, when a Far UV-C lamp is turned on), the ratio of the rates of ozone formation and decay will be much larger. Therefore, the potential exists for generation of O_3 from Far UV-C sources.

However, it is important to put this information into the proper context, specifically as it relates to Far UV-C sources. Continuing with the example of KrCl* sources, at 222 nm the absorption cross-section for O_2 is roughly 4 orders of magnitude lower than at 172 nm, the characteristic wavelength of a Xenon excimer lamp. Xenon excimer lamps are commonly used for O_3 generation because of the strong absorbance by O_2 of radiation at their characteristic emission wavelength, 172 nm. In fact, Xenon excimer lamps can be quite

efficient as O_3 generators. A KrCl* lamp will also generate O_3 photochemically, but the generation rate will be orders of magnitude lower than from a Xenon excimer lamp.

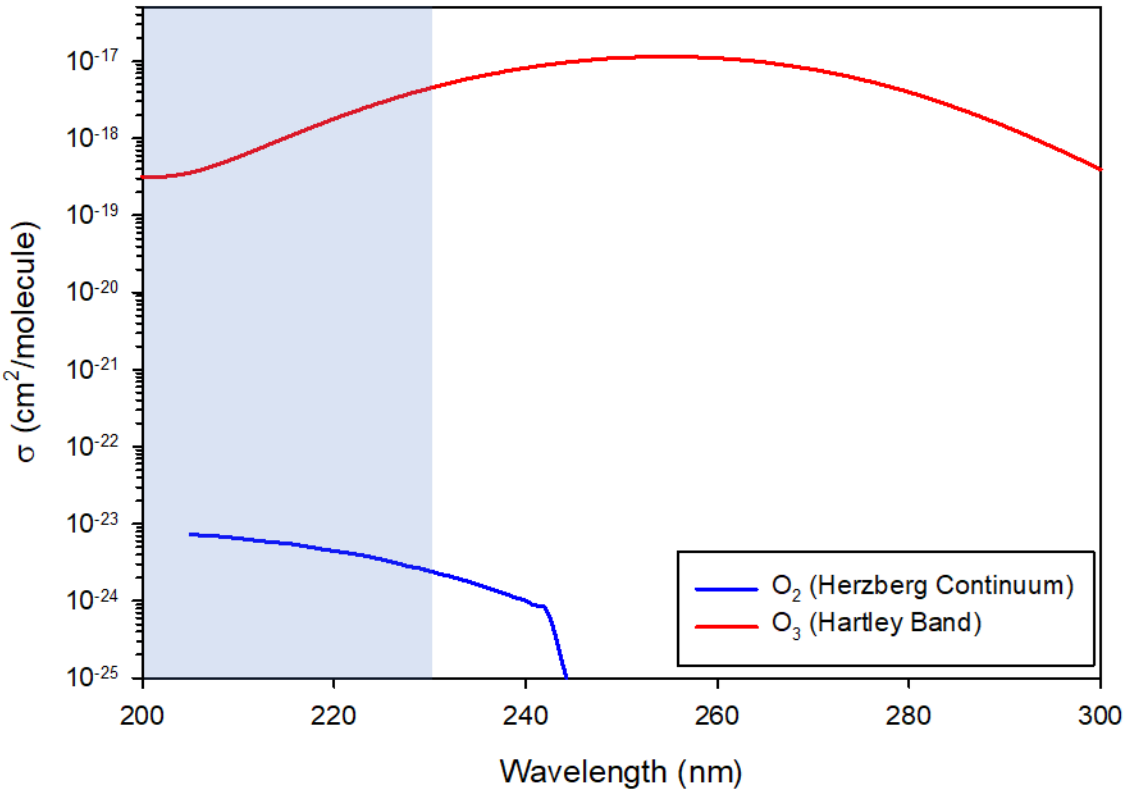

Figure 17. Absorption cross-sections for O_2 and O_3 for the wavelength rate 200 nm – 300 nm. Data from: *Chemical Kinetics and Photochemical Data for Use in Stratospheric Modeling, Evaluation Number 19*, JPL.[81] The shaded blue area indicates the Far UV-C range.

Generation of O_3 by a Far UV-C source will depend on the fundamental chemistry described above, but also local conditions of application. Relevant conditions will include the output power and output spectrum of the Far UV-C source, as well as air circulation and mixing in the vicinity of the lamp.

Additionally, it should be noted that excimer lamps, depending on power and design, are driven by voltages in the 2-10 kV range, which are applied to the outside of the lamp. At these high voltages there can be corona discharges on the exterior surface of the lamp. Since the discharge will happen in air, ozone generation rates by corona discharge can be an important contributor to ozone formation from a Far UV-C lamp and can be significantly higher than ozone generation by photochemical processes.

Ozone Generation Measurements

A "standard method" does not exist for measurement of O_3 production by Far UV-C lamps. As such, the development of a standard method represents a need.

For ozone-generating lamps, such as non-optically-filtered low-pressure Hg lamps (with a secondary line at 185 nm) or Xenon excimer lamps (peak output at 172 nm), ozone generation rates have been measured by inserting the lamp in a tube. The tube and lamp are flushed with a constant flow rate of gas (typically a nitrogen-oxygen mixture) under conditions of controlled humidity and temperature. Real-time

measurements of ozone concentration in the exhaust gas from this system are used to estimate ozone production rate by application of mass-balance principles.

Since KrCl* lamps (peak output at 222 nm) generate very small amounts of ozone and modern forms of such lamps are not cylindrical, the use of the approach described above becomes challenging. Beyond the geometric constraints of such a test, it is also difficult to accurately quantify the low concentrations of ozone (typically in the sub ppb_v range) at the exit of the tube.

For measurement of such low ozone generation rates, it is suggested to place the lamp into a relatively small (tens of liters) enclosed, well-mixed volume of air and measure the change of ozone concentration inside the volume as a function of time; mixing is necessary to overcome the tendency of O_3 to settle within the column of air. For such an experiment, it is critical to minimize or eliminate the presence of any reduced compounds in the enclosed vessel, as these compounds are likely to react rapidly with ozone, thereby skewing the results of the test. For that reason, the vessel should be constructed of materials that are non-reactive with ozone, such as glass or stainless steel. Time-course measurements of ozone concentration within the well-mixed chamber should be conducted using a calibrated ozone detector with resolution of at least 10 ppb_v.

Figure 18 illustrates example data sets from the protocol described above. Mass balance principles can be used to calculate the ozone production rate from the time-course ozone concentration measurements. Ozone production rate should be normalized with respect to lamp output power to allow calculation of an ozone generation index that could be used across a range of applications with one or many lamps.

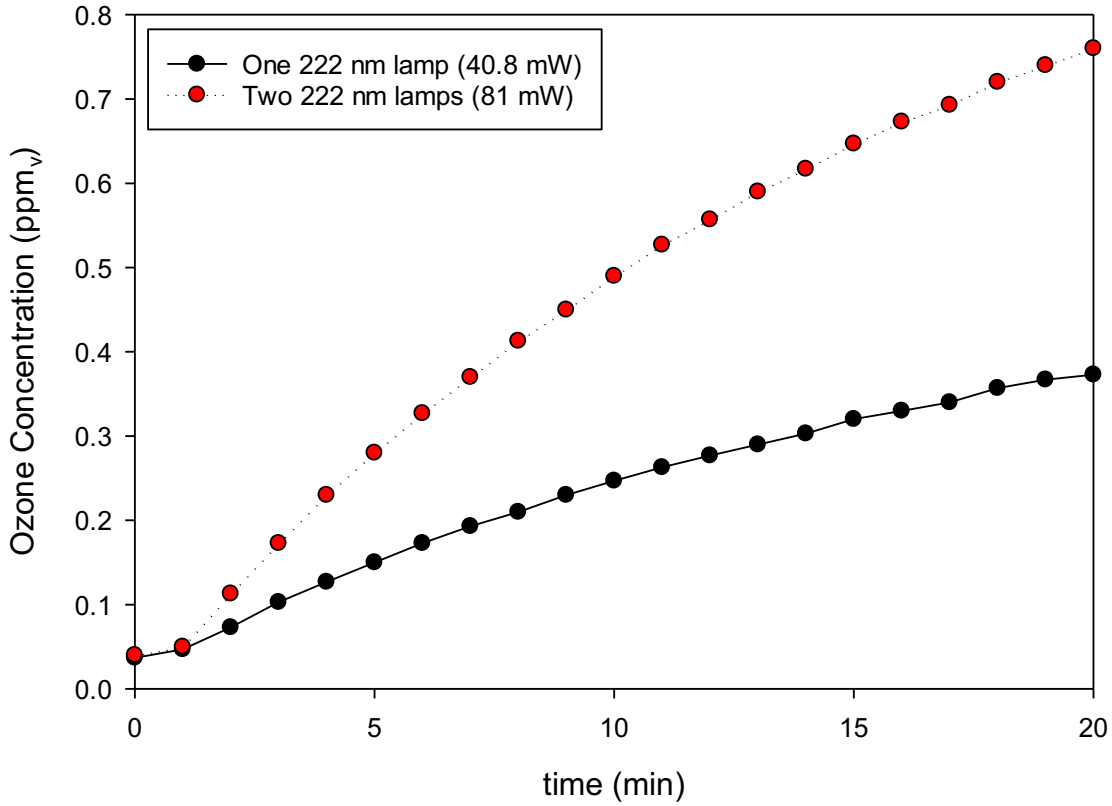

Figure 18. Example of time-course measurements of ozone concentration in a 35 L, well-mixed closed vessel with a single KrCl* lamp (40.8 mW output power) and two lamps (total of 81 mW output power).

As illustrated in Figure 18, the ozone concentration gradient decreases as ozone concentration increases, because of photochemical decay of ozone. Therefore, estimates of ozone generation rate from these lamps should be based on the initial, quasi-linear portion of the curve.

It is important to keep the data from Figure 18 in proper context. The measurements reported in Figure 18 were collected in a small, well-mixed, inert chamber with no air circulation. As such, these conditions are essentially optimized for accumulation of ozone from a Far UV-C lamp. In practical applications of these devices, air circulation from a conventional HVAC system can be used to maintain the ambient ozone concentration well below the limits that are presented in Table 2. By extension, this indicates that practical applications of Far UV-C sources should be developed by considering air circulation and mixing that is brought into an indoor air space by the existing HVAC system.

Two leading manufacturers of KrCl* lamps provided typical, measured ozone generation rates for their lamps. The lamps were operated at <12 W electrical power. The manufacturers reported significantly different generation rates of 85 µg/hour (9.4 µg O_3/W·hr) and 12 µg/hour (1.1 µg O_3/W·hr). One manufacturer also reported data for a 70 W lamp of 12 mg/hour (170 µg O_3/W·hr). It must be noted that the coaxial design of that lamp is quite different from the previously-mentioned low power lamps. The substantially higher ozone generation rate of this lamp is attributable to the contributions of corona discharges on the outside of the lamp, which led to much higher ozone generation than by just photochemical processes.

It is also worth noting that the methods used to measure ozone production from these lamps were different between the two manufacturers. The development of an industry standard for this measurement is needed to clarify the potential for ozone production in applications of Far UV-C sources.

Ozone Generation in Applications

Control of ozone exposure to humans and the environment will require that ozone generation rates from these lamps be quantified using a standardized method. Since the lamps will always be used in fixtures, it is the responsibility of the fixture manufacturer to provide data to customers about the ozone emission from the fixture.

For rough estimates of the room ozone concentration the following formula can be used:

$$\boldsymbol{Ozone\ Concentration} = \frac{\boldsymbol{Ozone\ Generation\ Rate} \times \boldsymbol{time}}{\boldsymbol{Room\ Volume}} \qquad (9)$$

Using one of the above-mentioned lamps (<12 W) as an example, ozone generation within a room of 1000 cubic feet (28.3 m^3 – standard room size for UL867) will be 0.034 ppm_v; such an installation would likely fall below the UL867 upper limit[82] of 0.050 ppm_v, particularly when "real world" conditions of air mixing and in/outflow are also considered. However, a larger installation (*e.g.*, 70 W lamp), an ambient concentration of 4.7 ppm_v would be expected.

Given the number of variables in lamp design, emission spectrum, lamp power, lamp duty cycle, room volume, air circulation, and air exchange rates, it is not possible to say whether a given Far UV-C installation presents an ozone risk without assessing its specifics. Ozone generation by current Far UV-C lamps must be discussed by fixture manufacturers and considered by those installing or managing these fixtures.

Conclusions

Based on the evidence in the published literature and the collation of expert knowledge by the authors, the following conclusions can be drawn:

- Far UV-C technology is currently dominated by one source type, the KrCl* lamp. Although alternate devices exist, they are not yet practically viable for disinfection applications.
- Though commonly referred to as 222 nm lamps, a KrCl* lamp will emit polychromatic radiation across a wide segment of the UV-C range; optical filters may be needed to limit substantial emissions to the Far UV-C range.
- Far UV-C is an effective viral disinfectant, with particular suitability as a technology response to transmission of SARS-CoV-2 via air and surfaces,
    - The efficacy of Far UV-C against viral pathogens is at least as high as that of conventional UVGI, and benefits from the long history of this technology as a disinfectant in a wide range of settings.
    - Absorption of UV-C radiation by dissolved constituents within aerosols or on solid surfaces will diminish the effectiveness of UV-C-based disinfection processes. The effects of UV-C absorption (and other optical processes) on UV-C disinfection efficacy for air and surfaces is understood qualitatively; development of a quantitative understanding of these effects is a research need.
    - Numerous non-pathogenic surrogate viruses (phages) are known that may enable validation test methodologies; however, selection of an appropriate surrogate will depend on the target virus and the wavelength(s) of UV-C radiation being applied.
- Solid photobiological principles underpin the hypothesis that Far UV-C radiation is less-damaging to mammalian tissues than longer-wavelength UV-C or UV-B radiation.
    - Evidence in support of this hypothesis has been mounting over the last decade, with an acceleration in interest since the emergence of the COVID-19 pandemic.
    - The predominant concern of skin carcinogenesis by UV exposure is misapplied in consideration of Far UV-C technology; a re-education on the photobiological connection between UV radiation and skin cancer is required.
    - Regulators and standards agencies on the global scale are monitoring the safety of this technology, and motion towards loosening restrictions on UV-C exposure (including Far UV-C) has already been observed.
- Ozone generation by Far UV-C sources is a due concern, resulting from photochemical and corona discharge processes,
    - The rate of ozone generation by these sources is orders of magnitude lower than for conventional “ozone generating” UV lamps.
    - Reasonable application of these sources for continuous, room-scale disinfection could be achieved while maintaining ozone concentrations below regulated values; however, it is also reasonable to consider applications where ambient ozone concentrations would exceed these values.
    - It is the responsibility of lamp manufacturers and those installing such systems to properly communicate and assess the potential ozone hazard of these systems.

Task Force Membership

The IUVA Task Force (TF) on Far UV-C Radiation for Disinfection of Air and Surfaces was formed with a goal of including expertise that spanned the three general issues described above: disinfection efficacy, safety of human exposure, and potential for ozone formation. Below is a list of TF members, each of whom contributed to the development of this white paper:

Ernest R. Blatchley III (TF Chair) is the Lee A. Rieth Professor in Environmental Engineering at Purdue University, where he holds a joint faculty appointment in the Lyles School of Civil Engineering and the Division of Environmental & Ecological Engineering. His research addresses theoretical and practical aspects of the use of UV radiation. Professor Blatchley serves as a member of the IUVA Board as well as Vice President for the Americas.

David Brenner is the Director of the Columbia University Center for Radiological Research. Founded by a student of Marie Curie, and focusing on new ways to use radiation to better human health, the Center is the oldest and largest radiation biology center in the US. He is also Director of the Columbia Radiological Research Accelerator Facility (RARAF), which is a national facility dedicated to probing the mechanisms underlying the biological effects of different radiations. Brenner is a recipient of the Failla gold medal, the annual award given by the Radiation Research Society for contributions to radiation research, and the Oxford University Weldon Prize for development of mathematical methods applied to problems in Biology.

Holger Claus (Chair, Ozone Generation Sub-Committee) is the Vice President of Technology at Ushio America Inc. Throughout his career he has developed and produced various kind of light sources, like fluorescent lamps, various kind of UV lamps, short arc Xenon, laser driven Xenon and super high pressure Mercury lamps, LED and laser products, and excimer lamps. Recently he has been leading the technical and regulatory efforts of Ushio America Inc. to introduce 222 nm lamps into the scientific community and the market.

Troy E. Cowan is the owner and founder of Vision Based Consulting, LLC, supporting clients in Federal program development and regulatory compliance tasks. Over the last four plus years, Troy has helped establish and facilitate the IUVA's 100 member Healthcare/UV Working Group, working towards the development of UV-C output and efficacy standards. As part of this effort, three international workshops have been delivered and multiple presentations made to IUVA, SPIE, ASHRAE and ISO on using UV-C to combat HAIs, with companion articles published in the Journals of Infection Control and Hospital Epidemiology, the SPIE Journal and UV Solutions on this critical issue.

Karl Linden (Chair, Disinfection Efficacy Sub-Committee) is a Professor of Environmental Engineering and the Mortenson Professor in Sustainable Development at the University of Colorado Boulder, USA. His research investigates novel water and wastewater treatment systems, including advanced and innovative UV systems for inactivation of pathogens and degradation of organic and other emerging contaminants. Linden served as 2019-2020 President of the Association of Environmental Engineering and Science Professors (AEESP) and 2013-2015 President of the International Ultraviolet Association (IUVA).

Yijing Liu (YP representative) is a second year Ph.D. student at the Ohio State University. She is working with Dr. Natalie Hull at the Water Treatment Engineering and Microbiome Research Group. She focuses on research related to the water microbiome, especially related to antibiotic resistant bacteria and opportunistic pathogens after ultraviolet (UV) treatments and the impacts on human health at the point of use.

Ted Mao is President, MW Technologies, Inc., offering "CTO for hire" to help start-up companies to develop and commercialize new technologies in the CleanTech space. He is currently an executive board

member of International UV Association (IUVA), Vice President of IUVA Americas and Coordinator of IUVA COVID-19 Task Force. Dr. Mao was Vice President, Research and Chief Technology Officer for 14 years at Trojan Technologies.

Sung-Jin Park is Chief Technology Officer and co-founder of Eden Park Illumination, Inc., and also an adjunct faculty in the Department of Electrical and Computer Engineering at the University of Illinois at Urbana-Champaign. His research and development work for the last 20 years have been focused on microplasma technology and science, including UV generation from microplasma lamps and their applications.

Patrick J (PJ) Piper is the Founder and CEO of Far UV Technologies, and served as PI for the company's NASA and AFWERX SBIR research and development contracts targeting foodborne illnesses and SARS-CoV-2 disinfection. Far UV Technologies has been rapidly commercializing 222nm Krypton Far UV disinfection ceiling lighting, floor lamp and handheld wand innovations, secured a broad technology and licensing agreement with Boeing, been awarded National Stock Numbers by the Department of Defense for Krypton Far UV solutions and is supporting multiple collaborative academic and industry Far UV research efforts and partnerships.

Rich Simons is Head of Application Science at AquiSense Technologies and has been developing UV-C LED systems for more than a decade; following a Ph.D. in water disinfection reactor design he has developed numerous UV products, and promotes the use of advanced technologies in system design. The core of Rich's work is to combine new and existing technologies in a way that extends their application space: the focus is less market disruption, and more market construction.

David Sliney (Chair, Safety Sub-Committee) served as the President of the American Society for Photobiology in 2008-2009, was Director of CIE Division 6 (Photobiology and Photochemistry), and he is Chair of the IES Photobiology Committee. He holds a Ph.D. in biophysics and medical physics from University College London, Institute of Ophthalmology. Dr. Sliney managed the Laser/Optical Radiation Program at what is now the Army Public Health Center until retiring in 2007. He is a faculty associate at the Johns Hopkins School of Public Health. His research interests focus on subjects related to ultraviolet effects upon the eye, photobiological hazards of intense optical sources and lasers, and optical safety of medical devices.

References

1. Sosnin, E. A.; Oppenlander, T.; Taranenko, V., Applications of capacitive and barrier discharge excilamps in photoscience. *J Photochem Photobiol C* **2006,** *7* (4), 145-63.
2. Tarasenko, V. F.; Sosnin, E. A., Barrier-discharge excilamps: History, operating principles, prospects. *J. Opt. Technol.* **2012,** *79* (10), 653-8.
3. Shuibov, A. K.; Shevera, I. V.; General, A., Low-pressure ultraviolet emitter utilizing chlorine and krypton chloride molecules. *High Temperature* **2004,** *42*, 875-8.
4. Zelikoff, M.; Wyckoff, P. H.; Achenbrand, L. M.; Loomis, R. S., Electrodeless discharge lamps containing metallic vapors. *J Opt Sci America* **1952,** *42* (11), 818-9.
5. Beck, S. E.; Wright, H. B.; Hargy, T. M.; Larason, T. C.; Linden, K. G., Action spectra for validation of pathogen disinfection in medium-pressure ultraviolet (UV) systems. *Water Res* **2015,** *70*, 27-37.
6. Kneissl, M., A Brief Review of III-Nitride UV Emitter Technologies and their applications. In *III-Nitride Ultraviolet Emitters*, Kneissl, M.; Rass, J., Eds. Springer: Switzerland, 2016.
7. Amano, H.; Collazo, R.; De Santi, C.; Einfeldt, S.; Funato, M.; Glaab, J.; Hagedorn, S.; Hirano, A.; Hirayama, H.; Ishii, R.; et_al., The 2020 UV emitter roadmap. *J. Phys. D: Appl. Phys.* **2020,** *53*, 503001.

8. Kneissl, M.; Seong, T. Y.; Han, J.; Amano, H., The emergence and prospects of deep-ultraviolet light-emitting diode technologies. *Nature Photonics* **2019,** *13*, 233-44.
9. Vuong, T. Q. P.; Cassabois, G.; Valvin, B.; Rousseau, E.; Summerfield, A.; Mellor, C. J.; Cho, Y.; Cheng, T. S.; Albar, J. D.; Eaves, L.; Fuxon, C. T.; Beton, P. H.; Novikov, S. V.; Gil, B., Deep ultraviolet emission in hexagonal boron nitride grown by high-temperature molecular beam epitaxy. *2D Materials* **2017,** *4*, 021023.
10. Zhao, S.; Lu, J.; Hai, X.; Yin, X., AlGaN nanowires for Ultraviolet light-emitting: Recent progress, challenges, and prospects. *Micromachines* **2020,** *11*, 125.
11. Harm, W., *Biological Effects of Ultraviolet Radiation*. Cambridge University Press: Cambridge, England, 1980.
12. Jagger, J., *Introduction to Research in Ultra-Violet Photobiology*. Prentice-Hall: Englewood Cliffs, N.J., 1967.
13. Beck, S. E.; Wright, H. B.; Hargy, T. M.; Larason, T. C.; Linden, K. G., Action spectra for validation of pathogen disinfection in medium-pressure ultraviolet (UV) systems. *Water Research* **2015,** *70*, 27-37.
14. Barancheshme, F.; Philiber, J.; Noam-Amar, N.; Gerchman, Y.; Barbeau, B., Assessment of saliva interference with UV-based disinfection technologies. *Journal of Photochemistry & Photobiology, B: Biology* **2021,** *217*, 112168.
15. Setlow, R.; Doyle, B., THE ACTION OF MONOCHROMATIC ULTRAVIOLET LIGHT ON PROTEINS. *Biochimica Et Biophysica Acta* **1957,** *24* (1), 27-41.
16. Voet, D.; Gratzer, W. B.; Cox, R. A.; Doty, P., ABSORPTION SPECTRA OF NUCLEOTIDES, POLYNUCLEOTIDES, AND NUCLEIC ACIDS IN THE FAR ULTRAVIOLET. *Biopolymers* **1963,** *1* (3), 193-208.
17. Lytle, C. D.; Sagripanti, J. L., Predicted inactivation of viruses of relevance to biodefense by solar radiation. *Journal of Virology* **2005,** *79* (22), 14244-14252.
18. Sagripanti, J. L.; Lytle, C. D., Estimated Inactivation of Coronaviruses by Solar Radiation With Special Reference to COVID-19. *Photochemistry and Photobiology* **2020,** *96* (4), 731-737.
19. Pendyala, B.; Patras, A.; Pokharel, B.; D'Souza, D., Genomic Modeling as an Approach to Identify Surrogates for Use in Experimental Validation of SARS-CoV-2 and HuNoV Inactivation by UV-C Treatment. *Frontiers in Microbiology* **2020,** *11*.
20. Rockey, N. C.; Henderson, J. B.; Chin, K.; Raskin, L.; Wigginton, K. R. Predictive modeling of virus inactivation by UV. https://www.biorxiv.org/content/10.1101/2020.10.27.355479v1.
21. Beck, S. E.; Hull, N. M.; Poepping, C.; Linden, K. G., Wavelength-Dependent Damage to Adenoviral Proteins Across the Germicidal UV Spectrum. *Environmental Science & Technology* **2018,** *52* (1), 223-229.
22. Beck, S. E.; Rodriguez, R. A.; Linden, K. G.; Hargy, T. M.; Larason, T. C.; Wright, H. B., Wavelength Dependent UV Inactivation and DNA Damage of Adenovirus as Measured by Cell Culture Infectivity and Long Range Quantitative PCR. *Environmental Science & Technology* **2014,** *48* (1), 591-598.
23. Linden, K. G.; Thurston, J.; Schaefer, R.; Malley, J. P., Enhanced UV inactivation of adenoviruses under polychromatic UV lamps. *Applied and Environmental Microbiology* **2007,** *73* (23), 7571-7574.
24. Blatchley III, E. R., Numerical modelling of UV intensity: Application to collimated-beam reactors and continuous-flow systems. *Water Research* **1997,** *31* (9), 2205-2218.
25. Bolton, J. R.; Linden, K. G., Standardization of methods for fluence (UV dose) determination in bench-scale UV experiments. *Journal of Environmental Engineering-Asce* **2003,** *129* (3), 209-215.
26. Welch, D.; Buonanno, M.; Grilj, V.; Shuryak, I.; Crickmore, C.; Bigelow, A. W.; Randers-Pehrson, G.; Johnson, G. W.; Brenner, D. J., Far-UVC light: A new tool to control the spread of airborne-mediated microbial diseases. *Scientific Reports* **2018,** *8*.
27. Chiu, K.; Lyn, D. A.; Savoye, P.; Blatchley, E. R., Integrated UV disinfection model based on particle tracking. *Journal of Environmental Engineering-Asce* **1999,** *125* (1), 7-16.

28. Lyn, D. A.; Chiu, K.; Blatchley, E. R., Numerical modeling of flow and disinfection in UV disinfection channels. *Journal of Environmental Engineering-Asce* **1999,** *125* (1), 17-26.
29. Naunovic, Z.; Lim, S.; Blatchley, E. R., Investigation of microbial inactivation efficiency of a UV disinfection system employing an excimer lamp. *Water Research* **2008,** *42* (19), 4838-4846.
30. Ahmed, Y. M.; Jongewaard, M.; Li, M. K.; Blatchley, E. R., Ray Tracing for Fluence Rate Simulations in Ultraviolet Photoreactors. *Environmental Science & Technology* **2018,** *52* (8), 4738-4745.
31. Ahmed, Y. M.; Ortiz, A. P.; Blatchley, E. R., Stochastic Evaluation of Disinfection Performance in Large-Scale Open-Channel UV Photoreactors. *Journal of Environmental Engineering* **2019,** *145* (10).
32. Ducoste, J. J.; Liu, D.; Linden, K., Alternative approaches to modeling fluence distribution and microbial inactivation in ultraviolet reactors: Lagrangian versus Eulerian. *Journal of Environmental Engineering-Asce* **2005,** *131* (10), 1393-1403.
33. Ducoste, J.; Linden, K.; Rokjer, D.; Liu, D., Assessment of reduction equivalent fluence bias using computational fluid dynamics. *Environmental Engineering Science* **2005,** *22* (5), 615-628.
34. Imoberdorf, G. E.; Taghipour, F.; Mohseni, M., Radiation field modeling of multi-lamp, homogeneous photoreactors. *Journal of Photochemistry and Photobiology a-Chemistry* **2008,** *198* (2-3), 169-178.
35. Sozzi, D. A.; Taghipour, F., UV reactor performance modeling by Eulerian and Lagrangian methods. *Environmental Science & Technology* **2006,** *40* (5), 1609-1615.
36. Buchan, A. G.; Yang, L.; Atkinson, K. D., Predicting airborne coronavirus inactivation by far-UVC in populated rooms using a high-fidelity coupled radiation-CFD model. *Scientific Reports* **2020,** *10* (1).
37. EPA, U. S., Ultraviolet Disinfection Guidance Manual for the Final Long Term 2 Enhanced Surface Water Treatment Rule. Water, O. o., Ed. Washington, DC, 2006.
38. Emerick, R. W.; Tchobanoglous, G. *Ultraviolet Disinfection Guidelines for Drinking Water and Water Reuse*; National Water Research Institute: Fountain Valley, CA, 2012.
39. ÖNORM, Devices for the disinfection of water using ultraviolet radiation Part 1: Devices equipped with UV low pressure lamps - Requirements and testing. Vienna, Austria, 2020; Vol. ÖNORM M 5873-1:2020.
40. ÖNORM, Plants for the disinfection of water using ultraviolet radiation—Requirements and testing—Part 2: Medium pressure mercury lamp plants. ÖNORM M 5873-2 ed.; Vienna, Austria, 2003.
41. ÖNORM, Devices for the disinfection of water using ultraviolet radiation Part 3: Reference radiometers for devices equipped with UV low pressure lamps - Requirements and testing. Vienna, Austria, 2020; Vol. ÖNORM M 5873-3:2020.
42. German; Standardization, I. f., Devices for the disinfection of water using ultraviolet radiation Part 1: Devices equipped with UV low pressure lamps - Requirements and testing. Berlin, Germany, 2020; Vol. DIN 19294-1:2020.
43. German; Standardization, I. f., Devices for the disinfection of water using ultraviolet radiation Part 3: Reference radiometers for devices equipped with UV low pressure lamps - Requirements and testing. Berlin, Germany, 2020; Vol. DIN 19294-3:2020.
44. Buonanno, M.; Ponnaiya, B.; Welch, D.; Stanislauskas, M.; Randers-Pehrson, G.; Smilenov, L.; Lowy, F. D.; Owens, D. M.; Brenner, D. J., Germicidal Efficacy and Mammalian Skin Safety of 222-nm UV Light. *Radiat. Res.* **2017,** *187* (4), 483-491.
45. Buonanno, M.; Randers-Pehrson, G.; Bigelow, A. W.; Trivedi, S.; Lowy, F. D.; Spotnitz, H. M.; Hammer, S. M.; Brenner, D. J., 207-nm UV light - a promising tool for safe low-cost reduction of surgical site infections. I: in vitro studies. *PLoS One* **2013,** *8* (10), e76968.
46. Buonanno, M.; Stanislauskas, M.; Ponnaiya, B.; Bigelow, A. W.; Randers-Pehrson, G.; Xu, Y.; Shuryak, I.; Smilenov, L.; Owens, D. M.; Brenner, D. J., 207-nm UV Light-A Promising Tool for

Safe Low-Cost Reduction of Surgical Site Infections. II: In-Vivo Safety Studies. *PLoS One* **2016,** *11* (6), e0138418.
47. Kaidzu, S.; Sugihara, K.; Sasaki, M.; Nishiaki, A.; Igarashi, T.; Tanito, M., Evaluation of acute corneal damage induced by 222-nm and 254-nm ultraviolet light in Sprague-Dawley rats. *Free Radic Res* **2019,** *53* (6), 611-617.
48. Fukui, T.; Niikura, T.; Oda, T.; Kumabe, Y.; Ohashi, H.; Sasaki, M.; Igarashi, T.; Kunisada, M.; Yamano, N.; Oe, K.; Matsumoto, T.; Matsushita, T.; Hayashi, S.; Nishigori, C.; Kuroda, R., Exploratory clinical trial on the safety and bactericidal effect of 222-nm ultraviolet C irradiation in healthy humans. *PLoS One* **2020,** *15* (8), e0235948.
49. Cadet, J., Harmless Effects of Sterilizing 222-nm far-UV Radiation on Mouse Skin and Eye Tissues. *Photochem Photobiol* **2020,** *96* (4), 949-950.
50. Barnard, I. R. M.; Eadie, E.; Wood, K., Further evidence that far-UVC for disinfection is unlikely to cause erythema or pre-mutagenic DNA lesions in skin. *Photodermatol Photoimmunol Photomed* **2020,** *36* (6), 476-477.
51. Hanamura, N.; Ohashi, H.; Morimoto, Y.; Igarashi, T.; Tabata, Y., Viability evaluation of layered cell sheets after ultraviolet light irradiation of 222 nm. *Regen Ther* **2020,** *14*, 344-351.
52. Yamano, N.; Kunisada, M.; Kaidzu, S.; Sugihara, K.; Nishiaki-Sawada, A.; Ohashi, H.; Yoshioka, A.; Igarashi, T.; Ohira, A.; Tanito, M.; Nishigori, C., Long-term Effects of 222-nm ultraviolet radiation C Sterilizing Lamps on Mice Susceptible to Ultraviolet Radiation. *Photochem Photobiol* **2020,** *96* (4), 853-862.
53. Hickerson, R. P.; Conneely, M. J.; Tsutsumi, S. K. H.; Wood, K.; Jackson, D. N.; Ibbotson, S. H.; Eadie, E., Minimal, superficial DNA damage in human skin from filtered far-ultraviolet-C (UV-C). *Br J Dermatol (2021)* https://doi.org/10.1111/bjd.19816.
54. Buonnano, M.; Welch, D.; Brenner, D. J., Exposure of human skin models to KrCl excimer lamps: The impact of optical filtering *Photochemistry and Photobiology (2021) In Press*.
55. Woods, J. A.; Evans, A.; Forbes, P. D.; Coates, P. J.; Gardner, J.; Valentine, R. M.; Ibbotson, S. H.; Ferguson, J.; Fricker, C.; Moseley, H., The effect of 222-nm UVC phototesting on healthy volunteer skin: a pilot study. *Photodermatol Photoimmunol Photomed* **2015,** *31* (3), 159-66.
56. Goldfarb, A. R.; Saidel, L. J., Ultraviolet absorption spectra of proteins. *Science* **1951,** *114* (2954), 156-7.
57. Setlow, J., The molecular basis of biological effects of ultraviolet radiation and photoreactivation. In *Current topics in radiation research*, M, E.; A, H., Eds. North Holland Publishing Company: Amsterdam, 1966; Vol. II, pp 195-248.
58. ACGIH *2021 TLVs and BEIs: Based on the Documentation of the Threshold Limit Values for Chemical and Physical Agents & Biological Exposure Indices*; American Conference of Governmental Industrial Hygienists: Cincinnati, OH, 2021.
59. Sliney, D., Balancing the Risk of Eye Irritation from UV-C with Infection from Bioaerosols. *Photochemistry and Photobiology* **2013,** *89* (4), 770-776.
60. Sliney, D. H.; Stuck, B. E., A Need to Revise Human Exposure Limits for Ultraviolet-C Radiation. *Photochemistry and Photobiology* **2021,** *97*, in press.
61. Organization, I. S., Photocarcinogenesis action spectrum (non-melanoma skin cancers). In *Standard ISO/CIE 28077:2016(E)*, ISO: Geneva, Switzerland, 2016.
62. (CIE), I. C. o. I. *UV-C Photocarcinogenesis Risks from Germicidal Lamps*; 2010.
63. Forbes, P. D.; Cole, C. A.; Forbes, P. D.; deGruijl, F., Origins and Evolution of Photocarcinogenesis Action Spectra, Including Germicidal UVC. **2020**.
64. Moan, J.; Grigalavicius, M.; Baturaite, Z.; Dahlback, A.; Juzeniene, A., The relationship between UV exposure and incidence of skin cancer. *Photodermatology Photoimmunology & Photomedicine* **2015,** *31* (1), 26-35.
65. Kaidzu, S.; Sugihara, K.; Sasaki, M.; Nishiakib, A.; Ohashi, H.; Igarashi, T.; Tanito, M., Re-evaluation of rat corneal damage by short wavelength UV revealed extremely less hazardous property of 222 nm-UV-C. *Private Communication, Under Peer Review* **2021**.

66. Pitts, D. G., The Human Ultraviolet Action Spectrum. *American Journal of Optometry and Physiological Optics* **1974,** *51*, 946-960.
67. Chaney, E. K.; Sliney, D. H., Re-evaluation of the ultraviolet hazard action spectrum-the impact of spectral bandwidth. *Health Physics* **2005,** *89* (4), 322-332.
68. Sliney, D. H., The Merits of an Envelope Action Spectrum for Ultraviolet Exposure Criteria. *American Industrial Hygiene Association Journal* **1972,** *32*, 415-431.
69. ICNIRP, Guidelines on limits of exposure to ultraviolet radiation of wavelengths between 180 nm and 400 nm (incoherent optical radiation). *Health Physics* **2004,** *87* (2), 171-186.
70. Richters, R. J.; Falcone, D.; Uzunbajakava, N. E.; Varghese, B.; Caspers, P. J.; Puppels, G. J.; van Erp, P. E.; van de Kerkhof, P. C., Sensitive Skin: Assessment of the Skin Barrier Using Confocal Raman Microspectroscopy. *Skin Pharmacol Physiol* **2017,** *30* (1), 1-12.
71. Lock-Andersen, J.; Therkildsen, P.; de Fine Olivarius, F.; Gniadecka, M.; Dahlstrom, K.; Poulsen, T.; Wulf, H. C., Epidermal thickness, skin pigmentation and constitutive photosensitivity. *Photodermatol Photoimmunol Photomed* **1997,** *13* (4), 153-8.
72. Tagami, H., Stratum Corneum Cell Layers. In *Textbook of Aging Skin*, Farage, M. A., Ed. Springer-Verlag: Berlin Heidelberg, 2015.
73. Segev, F.; Geffen, N.; Galor, A.; Cohen, Y.; Gefen, R.; Belkin, A.; Arieli, Y.; Epshtein, S.; Oren, A.; Harris, A., Dynamic assessment of the tear film muco-aqueous and lipid layers using a novel tear film imager (TFI). *Br J Ophthalmol* **2020,** *104* (1), 136-141.
74. NIOSH NIOSH Pocket Guide to Chemical Hazards. https://www.cdc.gov/niosh/npg/npgd0476.html.
75. EPA NAAQS Table. https://www.epa.gov/criteria-air-pollutants/naaqs-table.
76. Organization, W. H. Ambient (Outdoor) Air Pollution. https://www.who.int/news-room/fact-sheets/detail/ambient-(outdoor)-air-quality-and-health.
77. Chapman, S., A Theory of Upper-Atmospheric Ozone. *Memoirs of the Royal Meteorological Society* **1930,** *3* (26), 103-125.
78. Wayne, R. P., *Chemistry of Atmospheres*. Clarendon Press: Oxford, England, 1985.
79. Finlayson-Pitts, B. J.; Pitts, J. N. J., *Atmospheric Chemistry: Fundamentals and Experimental Technniques*. John Wiley & Sons: New York, 1986.
80. Stamnes, K., Radiation Transfer in the Atmosphere: Ultraviolet Radiation. In *Encyclopedia of Atmospheric Sciences*, 2nd ed.; North, G. R.; Pyle, J. A.; Zhang, F., Eds. Elsevier: Amsterdam, 2015; Vol. 5, pp 37-44.
81. Burkholder, J. B.; Sander, S. P.; Abbatt, J. P. D.; Barker, J. R.; Cappa, C.; Crounse, J. D.; T.S., D.; Huie, R. E.; Kolb, C. E.; Kurylo, M. J.; Orkin, V. L.; Percival, C. J.; Wilmouth, D. M.; Wine, P. H., Chemical Kinetics and Photochemical Data for Use in Atmospheric Studies. Jet Propulsion Laboratory, C. I. o. T., Ed. NASA: 2020; Vol. Evaluation Number 19.
82. Underwriters Laboratories, I., UL Standard for Safety for Electrostatic Air Cleaners. Northbrook, IL, 2000; Vol. UL 867, p 82.